Asunto: Acceptance of your submission to Macromolecular Reaction Engineering (mren.201400020R1) - [EMID:34e1cdfe5ea77b2e]
Fecha: 23-06-2014 09:04
Remitente: "Macromolecular Reaction Engineering" <no-reply@editorialmanager.com>
Destinatario: "Cecilia Fortunatti" <cfortunatti@plapiqui.edu.ar>
Responder a: "Macromolecular Reaction Engineering" <macromol@wiley-vch.de>

Dear Mrs. Fortunatti,

Thank you for submitting your revised manuscript "Modeling of RAFT Polymerization using Probability Generating Functions. Detailed Prediction of Full Molecular Weight Distributions and Sensitivity Analysis" to Macromolecular Reaction Engineering. The reviewer report and comments are included at the end of this email.

I'm pleased to inform you that your manuscript has been accepted for publication without change.

You do not need to send additional files at this time.

We will copyedit the accepted version of your manuscript and if we require any further information at this stage we will contact you. After copyediting we will let you know when you can expect to receive the proofs. Instructions for returning your proof corrections will be provided when the proofs are sent to you.

Open access publication of this work is possible via Wiley OnlineOpen, enabling you to meet institutional and funder open access mandates. Wiley OnlineOpen allows you to post the final, published PDF of your OnlineOpen article on your website, your institutional repository, or any other free public server straight away. The fee for OnlineOpen is US$3000. More information about Wiley OnlineOpen can be found at http://olabout.wiley.com/WileyCDA/Section/id-406241.html.

Congratulations on your results, and thank you for choosing Macromolecular Reaction Engineering for publishing your work. I hope you will consider us for the publication of your future manuscripts.

Yours sincerely,

Stefan Spiegel

PS If you believe your images might be appropriate for use on the cover of Macromolecular Reaction Engineering, and you would like your paper to be considered for the cover, please email us your layout suggestions with a short description. For details on cover image preparation please see the cover gallery on http://mre-journal.de/.

Macromolecular Reaction Engineering

# Modeling of RAFT Polymerization using Probability Generating Functions. Detailed Prediction of Full Molecular Weight Distributions and Sensitivity Analysis

--Manuscript Draft--

| | |
|---|---|
| **Manuscript Number:** | mren.201400020R1 |
| **Full Title:** | Modeling of RAFT Polymerization using Probability Generating Functions. Detailed Prediction of Full Molecular Weight Distributions and Sensitivity Analysis |
| **Article Type:** | Full Paper |
| **Section/Category:** | |
| **Keywords:** | modeling; molecular weight distribution (MWD); probability generating function (pgf); reversible addition fragmentation chain transfer (RAFT) |
| **Corresponding Author:** | Cecilia Fortunatti<br>PLAPIQUI<br>Bahía Blanca, Buenos Aires ARGENTINA |
| **Corresponding Author Secondary Information:** | |
| **Corresponding Author's Institution:** | PLAPIQUI |
| **Corresponding Author's Secondary Institution:** | |
| **First Author:** | Cecilia Fortunatti |
| **First Author Secondary Information:** | |
| **Order of Authors:** | Cecilia Fortunatti |
| | Claudia Sarmoria |
| | Adriana Brandolin |
| | Mariano Asteasuain |
| **Order of Authors Secondary Information:** | |
| **Abstract:** | A mathematical model of RAFT polymerization processes is presented capable of predicting the full molecular weight distribution (MWD) through the use of probability generating functions (pgf). The bivariate distribution of the intermediate RAFT species is calculated. The model is able to work with the three kinetic mechanisms currently under discussion for explaining the observed behavior of this type of polymerization. For comparison purposes, the population balances were also solved by direct integration of the resulting equations. The results show that the pgf technique allows obtaining accurate solutions with very small computational times for systems of any average molecular weight. Spurious oscillations observed in the high molecular weight tail of the MWD can be easily disregarded. A sensitivity analysis over several of the kinetic constants is also performed, showing the effects of changing their values over several orders of magnitude. This analysis aims to showcase the enormous potential of the pgf technique for modeling and optimization of complex polymerization kinetics. |
| **Additional Information:** | |
| **Question** | **Response** |
| Please submit a plain text version of your cover letter here.<br><br>Please note, if you are submitting a revision of your manuscript, there is an opportunity for you to provide your responses to the reviewers later; please do not add them to the cover letter. | Bahía Blanca, June 16th, 2014.<br><br>Dear<br>Editor, Macromolecular Reaction Engineering<br><br>Dear Sir,<br><br>Enclosed please find a copy of the revised version of the article that we submitted for publication in Macromolecular Reaction Engineering, entitled “Modeling of RAFT |

| | |
|---|---|
| | Polymerization using Probability Generating Functions. Detailed Prediction of Full Molecular Weight Distributions and Sensitivity Analysis," by Cecilia Fortunatti, Claudia Sarmoria, Adriana Brandolin and Mariano Asteasuain. We have addressed all of the referees' comments in an attached file.<br><br>We hope that you will find this revised work suitable for publication.<br><br>Sincerely yours,<br><br>Cecilia Fortunatti |

**Article type: Full Paper**

# Modeling of RAFT Polymerization using Probability Generating Functions. Detailed Prediction of Full Molecular Weight Distributions and Sensitivity Analysis

Cecilia Fortunatti,* Claudia Sarmoria, Adriana Brandolin, Mariano Asteasuain

_____

C. Fortunatti, Prof. C. Sarmoria, Prof. A. Brandolin, Prof. M. Asteasuain
Planta Piloto de Ingeniería Química (PLAPIQUI), UNS-CONICET, Camino La Carrindanga km 7, 8000 Bahía Blanca, Argentina
E-mail: cfortunatti@plapiqui.edu.ar

_____

A mathematical model of RAFT polymerization processes is presented capable of predicting the full molecular weight distribution (MWD) through the use of probability generating functions (pgf). The bivariate distribution of the intermediate RAFT species is calculated. The model is able to work with the three kinetic mechanisms currently under discussion for explaining the observed behavior of this type of polymerization. For comparison purposes, the population balances were also solved by direct integration of the resulting equations. The results show that the pgf technique allows obtaining accurate solutions with very small computational times for systems of any average molecular weight. Spurious oscillations observed in the high molecular weight tail of the MWD can be easily disregarded. A sensitivity analysis over several of the kinetic constants is also performed, showing the effects of changing their values over several orders of magnitude. This analysis aims to showcase the enormous potential of the pgf technique for modeling and optimization of complex polymerization kinetics.

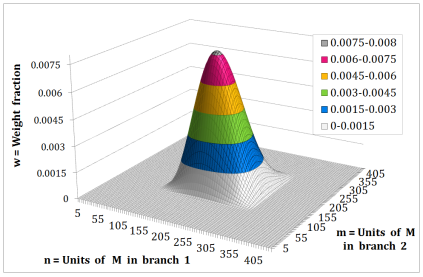


# 1. Introduction

The production of polymers of narrow molecular weight distribution is now feasible under industrial conditions using reversible-deactivation radical polymerization, which is commonly known as controlled radical polymerization or CRP. In this polymerization, a fast initiation step is followed by the establishment of a dynamic equilibrium between propagating radicals and various dormant species that is shifted towards the dormant species. As a result, the number of active chains at any given moment is several orders of magnitude smaller than that of the dormant species. Since each active chain may add only a few monomers before becoming dormant again, all chains grow slowly at approximately the same speed. Another consequence is that the rate of termination reactions is extremely low, since it depends on the concentration of active chains. For that reason, the fraction of dead chains is very small, and the reaction is practically “living”. Unlike conventional living ionic polymerizations, CRP allows the production of unique materials without stringent purity restrictions,[1] making this process interesting for industrial applications.

The three most successful CRP approaches are nitroxide-mediated polymerization (NMP), atom transfer radical polymerization (ATRP) and reversible addition-fragmentation chain transfer (RAFT). They differ in the type of agent used to establish the active-dormant species equilibrium and in the nature of this process. In this work we

focus on RAFT polymerization. This is one of the most versatile CRP techniques, highly effective in achieving the living behavior and compatible with a wide range of monomers.[2, 3] It is possible to use it for controlling molecular weights, molecular weight distributions, and even complex molecular architectures such as block and hyperbranched copolymers.[2, 4-7] On the down side, many RAFT transfer agents have limited commercial availability and low stability. In addition, some of them introduce end groups into the polymer that give it properties that could be undesirable for certain applications, such as color, smell or even toxicity. In those cases an extra step for removing them from the resin could be needed.[8]

As already mentioned, the different variants of CRP rely on establishing equilibria between active and dormant chains through the addition of an agent that can deactivate active chains reversibly. RAFT polymerization differs from the other CRP techniques in that the control on the growth of the polymer chains is achieved by means of a degenerative chain transfer process, instead of reversibly capping active radicals with a trapping agent. The RAFT agent adds to a living radical to produce an intermediate radical. This species can then undergo $\beta$-scission, either to liberate the living radical again or to produce a new living radical from the other end of the molecule. Any of these radicals continues the propagation reaction. The process rapidly converts the initial RAFT agent into a poly-RAFT agent, which in the addition reaction to living radicals generates a two-(polymeric) arm adduct. Eventually, the equilibrium is established between the addition and fragmentation reactions of the two-arm intermediate species.

Even though RAFT polymerizations have been studied extensively[2, 3, 9-16], there is an ongoing debate regarding particular aspects of the kinetic mechanism. It has been observed that for certain RAFT agents, such as dithiobenzoates and some

dithiocarbamates, there is rate retardation when the concentration of the RAFT agent is increased, as well as an induction period. This behavior is not expected for ordinary chain transfer agents.[9, 17] Three main theories have been developed to explain the different experimental findings for these systems:

Slow Fragmentation Theory (SF)

Barner-Kowollik et al.[18] proposed that the two-arm intermediate moiety is relatively stable and therefore fragments slowly, and that the termination reaction of this species is negligible. This theory predicts a large equilibrium constant for the active radical/two-arm RAFT intermediate species reaction, which is consistent with theoretical and experimental findings. However, a weak point of this theory is that it predicts concentrations for the two-arm adduct higher than the ones experimentally found.[16, 19]

Intermediate Radical Termination Theory (IRT)

Monteiro and de Brouwer[20] assumed that the two-arm adduct may cross-terminate with active radicals producing a dead three-arm star polymer. As a result of this reaction, the predicted equilibrium constant is much lower than in the SF model, while the overall radical concentration is consistent with experimental measurements. However, the IRT theory also predicts a population of three-arm star polymers that is much higher than the one experimentally detected.[16, 19]

Intermediate Radical Termination with Oligomers Theory (IRTO)

More recently, Konkolewicz et al.[2] developed a theory that considers that the RAFT adduct may cross-terminate, but only with short active radicals up to two monomers in length. The equilibrium constant and two-arm species concentrations, as well as the

amount of three-arm star polymers predicted by this theory, are all in agreement with experimental studies. The authors argue that long chain radicals diffuse slowly and experience steric hindrance around the radical center, rendering them unable to cross-terminate with the adduct.[16, 19]

There are other proposed mechanisms in the literature. For instance, Buback et al.[12] proposed that the star product resulting from cross-termination could undergo secondary reactions with propagating radicals. This "missing step" theory could account for the low concentration of star polymer in RAFT. Moreover, Meiser and Buback[21] recently isolated some of the expected by-products of these so called "missing steps."

An extensive review on the proposed mechanisms and causes of retardation in dithio-benzoate-mediated RAFT systems has been developed by Moad,[22] where more specific details of the kinetic discussion can be found.

Interpretation of experimental data using the three main different theories (SF, IRT and IRTO) has led to values of rate constants that may differ in up to six orders of magnitude.[23, 24] General agreement about the actual mechanism of RAFT polymerization is far from having been reached. Actually, active research is being carried out on the discrimination between RAFT kinetic theories. Recent works provided evidence that the IRT theory provides the best explanation for the rate retardation observed in polystyryl dithiobenzoate-mediated styrene polymerization.[25] On the other hand, Ting et al.[26] provided experimental evidence that is consistent with the IRTO theory. In this context, comprehensive mathematical models may be a very important tool to aid in the discrimination between the competing theories. They may also be useful for the design of experiments, the optimization of the reaction and the scaling up of the polymerization process.

Several studies have addressed the modeling and simulation of RAFT systems based on the proposed mechanisms. Most of them involved the prediction of average properties using the method of moments. For instance, Zhang and Ray[3, 27] developed a mathematical model that was employed in analyzing process development and design issues. Wang and Zhu[28-30] carried out a comprehensive analysis of the kinetics and polymer chain properties. More recently, Ye and Schork[31] used moment equations to develop a chain and sequence model suitable for optimizing the feeding policy in order to obtain a pre-specified polymer microstructure.

Other authors developed models of RAFT processes capable of predicting the full MWD using the PREDICI commercial software.[18, 32-34] In 2001, Barner-Kowollik et al.[18] used this software for determining rate coefficients associated with the addition-fragmentation equilibrium by careful modeling of the time-dependent evolution of experimental MWDs. Later on, Feldermann et al.[32] carried out simulations of a RAFT polymerization showing results consistent with the SF theory. On the same path, Pallares et al.[33] developed a mathematical model based on moment equations able to describe a complete mechanism that included the two-arm adduct cross-termination, thermal self-initiation of monomer and chain transfer reactions. The resulting mathematical model was solved using both FORTRAN and PREDICI commercial software, finding equivalent predictions.

The version of PREDICI used by Pallares et al.[33] required the use of two one dimensional (1D) polymer populations, a strategy whose accuracy has been questioned.[35] Nevertheless, several authors have proved that this simplification could properly represent the kinetics and MWD of the propagating radicals and one arm dormant species.[33, 36] However, the information on how the two arms of the RAFT adduct are interconnected is lost in the 1D PREDICI scheme which makes impossible

the obtainment of its full two dimensional (2D) MWD.[37] It has been reported that a module with 2D arrays has been added to PREDICI to overcome this limitation.[38] Using a different approach, Konkolewicz et al.[2] modeled the full MWD of RAFT polymers according to the IRTO theory assuming a priori knowledge of the shape of the distribution. They found good agreement with experimental data. In a more recent work,[39] they developed a simple mathematical model using assumptions such as linear dependency of molecular weight with conversion, in order to fit experimental values of conversion, molecular weight and polydispersity index (PDI) to validate the proposed mechanism. Konkolewicz et al.[19] have also simplified their first model so that the polymerization behavior depends on two parameters only. The simplified mathematical model showed good agreement with experimental MWD of several RAFT oligomers. Tobita[24, 40] modeled average properties and the full MWD of RAFT polymers and studied the influence of particle size on polymerization rate in mini-emulsion systems, employing probabilistic methods and relying on simplifying assumptions.

Both Konkolewicz[2] and Tobita[24] based their models on the fact that a living radical polymerization progresses by multiple uncapping-recapping events, and that chain growth only occurs between uncapping and recapping. Given that the probability of adding a monomeric unit during these events is small, a reasonable approximation of the distribution of radical lengths was used. Even though good agreement with experimental data was found, these simplifications can limit the potential of the mathematical model.

Monte Carlo methods have also been used to model RAFT reactions. Prescott[41] developed a Monte Carlo model to determine the role of chain-length dependent termination in RAFT systems. Afterwards, Prescott et al.[42] used this model to find ways to improve polymerization rates in RAFT emulsion polymerizations. Furthermore,

Chaffey-Millar et al.[43] presented a novel, parallelized approach to Monte Carlo simulation able to deal with complex kinetic schemes while providing detailed information on polymer microstructure. They reported computing times shorter than those necessary when using PREDICI.

Other authors have modeled rigorously the full MWD in RAFT processes by solving the complete set of population balances.[33] Zapata-González et al.[16] presented a comprehensive analysis of the full MWD and average properties for the three main kinetic mechanisms proposed in the literature using direct integration. The drawback of this approach is its high computational cost due to the large number of equations to be solved. By the use of the quasi-steady-state approximation, the authors reduced the stiffness of the system of equations. This approximation allowed shortening the time necessary to solve the differential algebraic equation (DAE) system. The difficulty in model development and execution time increases in the case of copolymerization processes and / or prediction of complex molecular architectures.

In spite of these efforts, further improvement of RAFT models is still needed. A particular feature of RAFT systems that makes their modeling difficult is the bivariate nature of the MWD of the two-arm intermediate species. This is an adduct of two growing polymer chains, temporarily linked to the RAFT agent. The 2D treatment is the only way of knowing how the two arms are interlinked. Knowledge on the full MWD of the intermediate adduct could aid in analyzing the different proposed mechanisms for RAFT polymerization[16] and accurately predict the behavior of the system in the case of side reactions involving the two-arm adduct.[9] Zapata-González et al.[37] claimed to obtain the full 2D MWD of the two-arm adduct radicals but only the 1D MWD is reported in their work. Taking into consideration that the 1D distribution is based on the

total length of the two-arm intermediate, the information of the length of each individual arm is lost.

In previous works, a mathematical model of a RAFT polymerization system that follows the SF kinetics was developed.[44] This mathematical model was capable of predicting not only the average properties but also the full MWD of the polymer by means of the probability generating function (pgf) transform. This technique allowed obtaining reliable outcomes with small computational resources.

In this work, the previous model has been extended to simulate the RAFT polymerization according to either SF, IRT or IRTO kinetics. Comments on the computational efficiency and numerical behavior of the pgf technique are presented. Besides, prediction of the bivariate MWD of the intermediate two-arm adduct is reported. In addition, a sensitivity analysis of controversial rate constants was performed aiming at studying their influence on the model predictions and showcasing the pgf technique versatility.

## 2. Methods

### 2.1 Kinetic Mechanism

The mathematical model is based on the kinetic mechanism indicated by equations 1-9. Please note that by setting appropriate values to the kinetic constants, it is possible to represent the three theories for explaining the RAFT phenomena that were discussed in the Introduction.

Initiation: $$\mathrm{I} \xrightarrow{f \quad k_\mathrm{d}} 2\,\mathrm{R}_0 \tag{1}$$

Propagation: $$\mathrm{R}_n + \mathrm{M} \xrightarrow{k_\mathrm{p}} \mathrm{R}_{n+1} \quad n = 0,\ldots,\infty \tag{2}$$

*Pre equilibrium*

Addition: $$\mathrm{R}_n + \mathrm{TR}_0 \xrightarrow{k_{a1}} \mathrm{R}_n\mathrm{TR}_0 \quad n = 0,\ldots,\infty \tag{3}$$

Fragmentation: $$\mathrm{R}_n\mathrm{TR}_0 \xrightarrow{k_{f1}} \mathrm{TR}_p + \mathrm{R}_q \quad p,q = n,0 \text{ or } 0,n \quad n = 0,\ldots,\infty \tag{4}$$

*Core equilibrium*

Addition: $$\mathrm{R}_n + \mathrm{TR}_m \xrightarrow{k_a} \mathrm{R}_n\mathrm{TR}_m \quad n = 0,\ldots,\infty \quad m = 1,\ldots,\infty \tag{5}$$

Fragmentation: $$\mathrm{R}_n\mathrm{TR}_m \xrightarrow{k_f} \mathrm{TR}_p + \mathrm{R}_q \quad p,q = n,m \text{ or } m,n \quad n = 0,\ldots,\infty \quad m = 1,\ldots,\infty \tag{6}$$

Termination by combination: $$\mathrm{R}_n + \mathrm{R}_m \xrightarrow{k_{tc}} \mathrm{P}_{n+m} \quad n,m = 0,\ldots,\infty \tag{7}$$

Termination by disproportionation: $$\mathrm{R}_n + \mathrm{R}_m \xrightarrow{k_{td}} \mathrm{P}_n + \mathrm{P}_m \quad n,m = 0,\ldots,\infty \tag{8}$$

Cross-termination:

$$R_s + R_nTR_m \xrightarrow{k_c} P_{n+m+s} \quad n, m = 0,\ldots,\infty$$

the length of radical chain is $$\begin{cases} \text{IRT}: & s = 0,\ldots,\infty \\ \text{IRTO}: & s = 0,1,2 \end{cases} \tag{9}$$

The chemical species involved are: initiator (I), monomer (M), active radicals with $n$ units of M ($R_n$), dormant (inactive) radicals with $n$ units of M ($TR_n$), intermediate (adduct) radicals with two arms of different length ($R_nTR_m$), and terminated (dead) polymer chains of length $n$ ($P_n$). The chain transfer agent (CTA) is regarded as an inactive radical with 0 units of monomer ($TR_0$). For simplicity, a single set of constants was used for both the pre-equilibrium and the core equilibrium ($k_{a1} = k_a$, $k_{f1} = k_f$). Nevertheless, applying the methodology using different sets of constants for the two equilibriums would be straightforward.

Given the theoretical nature of this work, a set of typical values taken from the literature was used for each kinetic mechanism being considered. The values used as reference for

the kinetic parameters are shown in Table 1. Unless otherwise noted, those values are applicable to the three kinetic schemes.

*Table 1*. Reference kinetic parameters.[16]

| **Reaction** | **Parameter** | **Units** |
|---|---|---|
| Initiation | $f = 0.5$ | |
| | $k_d = 0.036$ | $h^{-1}$ |
| Propagation | $k_p = 3.6 \times 10^6$ | $L \cdot mol^{-1} \cdot h^{-1}$ |
| Addition | $k_a = 3.6 \times 10^9$ | $L \cdot mol^{-1} \cdot h^{-1}$ |
| Fragmentation | *SF theory:* $k_f = 36$ | $h^{-1}$ |
| | *IRT & IRTO theories:* $k_f = 3.6 \times 10^7$ | $h^{-1}$ |
| Termination by combination | $k_{tc} = 3.6 \times 10^{10}$ | $L \cdot mol^{-1} \cdot h^{-1}$ |
| Termination by disproportionation | $k_{td} = 3.6 \times 10^{10}$ | $L \cdot mol^{-1} \cdot h^{-1}$ |
| Cross-termination | *SF theory:* $k_c = 0$ | $L \cdot mol^{-1} \cdot h^{-1}$ |
| | *IRT & IRTO theories:* $k_c = 3.6 \times 10^{10}$ | $L \cdot mol^{-1} \cdot h^{-1}$ |

### 1.1. Modeling of Average Properties

The mathematical model development is based on the population balances drawn from the kinetic mechanism. The well-known method of moments is used to transform these balances for modeling average molecular properties. The moments involved in the mathematical model are defined below:

*Moment of order a (a = 0, 1, 2) of active radicals:*

$$\lambda_a = \sum_{n=0}^{\infty} n^a \left[ R_n \right] \tag{10}$$

*Moment of order a (a = 0, 1, 2) of dormant radicals of one arm:*

$$\mu_a^I = \sum_{n=0}^{\infty} n^a \left[TR_n\right] \tag{11}$$

*Moment of order a,b (a,b = 0,0; 1,0; 0,1; 2,0; 1,1; 0,2) of two-arm adduct radicals considering the length of each arm:*

$$\mu_{a,b}^{II} = \sum_{n=0}^{\infty}\sum_{m=0}^{\infty} n^a m^b \left[R_n TR_m\right] \tag{12}$$

*Moment of order a (a = 0, 1, 2) of adduct radicals considering their total length:*

$$\mu_a^{II} = \sum_{n=0}^{\infty} n^a \left[\left(RTR\right)_n\right] \tag{13}$$

where *n* is the total chain length of the two-arm adduct.

*Partial moment of order 0 of two-arm adduct radicals:*

$$d\,\mu_{0\ n}^{II} = \sum_{s=0}^{\infty}\left[R_n TR_s\right] \tag{14}$$

*Moment of order a (a = 0, 1, 2) of dead polymer chains:*

$$\varepsilon_a = \sum_{n=0}^{\infty} n^a \left[P_n\right] \tag{15}$$

The population balances are:

*Initiator:*

$$\frac{d}{dt}\left(\left[I\right]\right) = -k_{\mathrm{d}}\left[I\right] \tag{16}$$

*Monomer:*

$$\frac{d}{dt}\left(\left[M\right]\right) = -k_{\mathrm{p}}\left[M\right]\lambda_0 \tag{17}$$

*Living radicals with n units of monomer (n = 0,..., ∞):*

$$\begin{aligned}\frac{d}{dt}\left(\left[R_n\right]\right) = {} & 2\,f\,k_{\mathrm{d}}\left[I\right]\delta_{n,0} + k_{\mathrm{p}}\left[M\right]\left[R_{n-1}\right]\left(1-\delta_{n,0}\right) + \left(\tfrac{1}{2}\right)k_{\mathrm{f}}\,d\,\mu_{0\ n}^{II} \\ & -\left(\begin{array}{l} k_{\mathrm{p}}\left[M\right] + k_{\mathrm{a}}\mu_0^I + \left(k_{\mathrm{tc}} + k_{\mathrm{td}}\right)\lambda_0 \\ +k_{\mathrm{c}}\mu_0^{II}\left(\left(\delta_{n,0}+\delta_{n,1}+\delta_{n,2}\right)\delta_{\mathrm{theory,IRTO}} + \delta_{\mathrm{theory,IRT}}\right)\end{array}\right)\left[R_n\right]\end{aligned} \tag{18}$$

*Dormant radicals of one arm with n units of monomer (n = 0,..., ∞):*

$$\frac{d}{dt}\left(\left[TR_n\right]\right) = -k_a \lambda_0 \left[TR_n\right] + \left(\tfrac{1}{2}\right) k_f \, d\mu_{0\,n}^{II} \tag{19}$$

*Two-arm adduct radicals with arms of length n and m (n, m = 0,..., ∞):*

$$\begin{aligned}\frac{d}{dt}\left(\left[R_n TR_m\right]\right) = &-\left(k_f + k_c\left(\lambda_0\, \delta_{\text{theory, IRT}} + \left(\left[R_0\right] + \left[R_1\right] + \left[R_2\right]\right)\delta_{\text{theory, IRTO}}\right)\right)\left[R_n TR_m\right] \\ &+ k_a\left(\left[R_n\right]\left[TR_m\right] + \left[R_m\right]\left[TR_n\right]\right)\end{aligned} \tag{20}$$

*Intermediate (adduct) radicals with two arms and total length n (n = 0,..., ∞):*

$$\begin{aligned}\frac{d}{dt}\left(\left[RTR_n\right]\right) = &-\left(k_f + k_c\left(\lambda_0\, \delta_{\text{theory, IRT}} + \left(\left[R_0\right] + \left[R_1\right] + \left[R_2\right]\right)\delta_{\text{theory, IRTO}}\right)\right)\left[RTR_n\right] \\ &+ k_a \sum_{i=0}^{n}\left(\left[R_{n-i}\right]\left[TR_i\right]\right)\end{aligned} \tag{21}$$

*Partial moment of order zero of adduct radicals (n = 0,..., ∞):*

$$\begin{aligned}\frac{d}{dt}\left(d\mu_{0\,n}^{II}\right) = &-\left(k_f + k_c\left(\lambda_0\, \delta_{\text{theory, IRT}} + \left(\left[R_0\right] + \left[R_1\right] + \left[R_2\right]\right)\delta_{\text{theory, IRTO}}\right)\right) d\mu_{0\,n}^{II} \\ &+ k_a\left(\lambda_0\left[TR_n\right] + \mu_0^I\left[R_n\right]\right)\end{aligned} \tag{22}$$

*Terminated (dead) polymer chains of length n (n = 0,..., ∞):*

$$\begin{aligned}\frac{d}{dt}\left(\left[P_n\right]\right) = &\, k_{td}\lambda_0\left[R_n\right] + \left(\tfrac{1}{2}\right) k_{tc}\sum_{i=0}^{n}\left(\left[R_{n-i}\right]\left[R_i\right]\right) + k_c\sum_{i=0}^{n}\left(\left[R_{n-i}\right]\left[\left(RTR\right)_i\right]\right)\delta_{\text{theory, IRT}} \\ &+ k_c\sum_{i=0}^{2}\left(\left[R_i\right]\left[\left(RTR\right)_{n-i}\right]\right)\delta_{\text{theory, IRTO}}\end{aligned} \tag{23}$$

In these equations, $\delta_{\text{theory, }theorytype}$ is 1 if theory = *theorytype* and 0 otherwise.

The moment equations are:

*Moment of order a (a = 0, 1, 2) of living radicals:*

$$\begin{aligned}\frac{d}{dt}\left(\lambda_a\right) = &\, 2 f\, k_d\left[I\right](0)^a + k_p\left[M\right]\sum_{j=0}^{a}\binom{a}{j}\lambda_j - k_c\mu_0^{II}\left(0^a\left[R_0\right] + 1^a\left[R_1\right] + 2^a\left[R_2\right]\right)\delta_{\text{theory, IRTO}} \\ &+ \left(\tfrac{1}{2}\right) k_f\,\mu_{a,0}^{II} - \left(k_p\left[M\right] + k_a\mu_0^I + \left(k_{tc} + k_{td}\right)\lambda_0 + k_c\mu_0^{II}\,\delta_{\text{theory, IRT}}\right)\lambda_a\end{aligned} \tag{24}$$

*Moment of order a (a = 0, 1, 2) of dormant radicals of one arm:*

$$\frac{d}{dt}\left(\mu_a^I\right) = -k_a \lambda_0 \mu_a^I + \left(\tfrac{1}{2}\right) k_f \ \mu_{a,0}^{II} \tag{25}$$

*Moment of order a,b (a,b = 0,0; 1,0; 0,1; 2,0; 1,1; 0,2) of two arms adduct radicals considering the length of each arm:*

$$\begin{aligned}\frac{d}{dt}\left(\mu_{a,b}^{II}\right) = &-\left(k_f + k_c\left(\lambda_0\ \delta_{\text{theory, IRT}} + \left(\left[R_0\right]+\left[R_1\right]+\left[R_2\right]\right)\delta_{\text{theory, IRTO}}\right)\right)\mu_{a,b}^{II} \\ &+ k_a\left(\lambda_a\ \mu_b^I + \lambda_b\ \mu_a^I\right)\end{aligned} \tag{26}$$

*Moment of order a (a = 0, 1, 2) of adduct radicals considering their total length:*

$$\begin{aligned}\frac{d}{dt}\left(\mu_a^{II}\right) = &-\left(k_f + k_c\left(\lambda_0\ \delta_{\text{theory, IRT}} + \left(\left[R_0\right]+\left[R_1\right]+\left[R_2\right]\right)\delta_{\text{theory, IRTO}}\right)\right)\mu_a^{II} \\ &+ k_a \sum_{j=0}^{a}\binom{a}{j}\lambda_{a-j}\ \mu_j^I\end{aligned} \tag{27}$$

*Moment of order a (a = 0, 1, 2) of dead polymer chains ($P_n$):*

$$\begin{aligned}\frac{d}{dt}\left(\varepsilon_a\right) = &\ k_{td}\lambda_0\ \lambda_a + \left(\tfrac{1}{2}\right)k_{tc}\sum_{j=0}^{a}\binom{a}{j}\lambda_{a-j}\ \lambda_j + k_c\left\{\sum_{j=0}^{a}\binom{a}{j}\lambda_{a-j}\ \mu_j^{II}\right\}\delta_{\text{theory, IRT}} \\ &+ k_c\left\{\sum_{j=0}^{a}\binom{a}{j}\left(0^j\left[R_0\right]+1^j\left[R_1\right]+2^j\left[R_2\right]\right)\mu_{a-j}^{II}\right\}\delta_{\text{theory, IRTO}}\end{aligned} \tag{28}$$

### 1.2. Modeling the Full MWD

The probability generating function (pgf) technique is employed to model the full MWD of the polymer. This technique consists in transforming the mass balances of polymeric species, characterized by the number of monomer units, to the pgf domain, producing as a result balances for the pgf transform of the MWD. Discrete points of the full MWD are recovered from the pgf domain by applying an appropriate numerical inversion technique.[45, 46] It is important to point out that this method does not require any prior knowledge of the shape of the MWD, and can deal with complex kinetic mechanisms.

A combination of univariate[46] and bivariate[45] pgfs are applied to the population balances to model the MWD of the different polymeric species.

The univariate pgf of order $a$ ($\vartheta_a = \phi_a,\ \varphi_a^I, \varphi_a^{II}, \chi_a$) of any species $X_n$ ($X_n = R_n, TR_n, (RTR)_n, P_n$) is defined as follows:

$$\vartheta_a(z) = \sum_{n=0}^{\infty} z^n n^a \frac{[X_n]}{\gamma_a} \tag{29}$$

where z is the dummy variable of the pgf and $\gamma_a$ is the moment of order $a$ of species $X_n$ ($\gamma_a = \lambda_a,\ \mu_a^I,\ \mu_a^{II},\ \varepsilon_a$). The bivariate pgf of order $a,b$ ($\psi_{a,b}$) of species $R_nTR_m$ is defined as follows:

$$\psi_{a,b}(z, w) = \sum_{n=0}^{\infty} z^n n^a \sum_{m=0}^{\infty} w^m m^b \frac{[R_n TR_m]}{\mu_{a,b}^{II}} \tag{30}$$

where $z$ and $w$ are the dummy variables of the pgf. In this work only pgf of order 0 will be employed. Univariate pgf transform is applied to the population balances of the species described by a univariate distribution ($R_n$, $TR_n$, $(RTR)_n$, $P_n$), and bivariate pgfs are used in the case of $R_nTR_m$. Details about the transformation process can be found elsewhere.[47, 48] The corresponding pgf balance equations are shown below:

*Univariate pgf of order 0 of active radicals ($\phi_0$):*

$$\begin{aligned}\frac{d}{dt}\left(\lambda_0\phi_0(z)\right) = {} & 2f\,k_{\mathrm{d}}[I] + k_{\mathrm{p}}[M]\left[z\left(\lambda_0\phi_0(z)\right) - \left(\lambda_0\phi_0(z)\right)\right] - k_{\mathrm{a}}\,\mu_0^I\left(\lambda_0\phi_0(z)\right) \\ & + \left(\frac{1}{2}\right)k_{\mathrm{f}}\left(\mu_{00}^{II}\varphi_{00}^{II}(z,1)\right) - \left(k_{\mathrm{tc}} + k_{\mathrm{td}}\right)\lambda_0\left(\lambda_0\phi_0(z)\right) \\ & - k_{\mathrm{c}}\,\mu_0^{II}\left\{\left(\lambda_0\phi_0(z)\right)\delta_{\text{theory, IRT}} + \left([R_0] + z[R_1] + z^2[R_2]\right)\delta_{\text{theory, IRTO}}\right\}\end{aligned} \tag{31}$$

*Univariate pgf of order 0 of dormant radicals of one arm ($\varphi^I_0$):*

$$\frac{d}{dt}\left(\mu_0^I\varphi_0^I(z)\right) = -k_{\mathrm{a}}\,\lambda_0\left(\mu_0^I\varphi_0^I(z)\right) + \left(\frac{1}{2}\right)k_{\mathrm{f}}\left(\mu_{00}^{II}\varphi_{00}^{II}(z,1)\right) \tag{32}$$

*Univariate pgf of order 0 of two-arm adduct radicals considering their total length ($\varphi^{II}_0$):*

$$\frac{d}{dt}\left(\mu_0^{II}\varphi_0^{II}(z)\right) = k_a\left(\lambda_0\phi_0(z)\right)\left(\mu_0^{I}\varphi_0^{I}(z)\right) - k_f\left(\mu_0^{II}\varphi_0^{II}(z)\right) - k_c\left\{\lambda_0\left(\mu_0^{II}\varphi_0^{II}(z)\right)\delta_{\text{theory, IRT}} + \left(\left[R_0\right]+\left[R_1\right]+\left[R_2\right]\right)\left(\mu_0^{II}\varphi_0^{II}(z)\right)\delta_{\text{theory, IRTO}}\right\} \quad (33)$$

*Univariate pgf of order 0 of terminated polymer chains $P_n$ ($\chi_0$):*

$$\frac{d}{dt}\left(\varepsilon_0\chi_0(z)\right) = k_{td}\lambda_0\left(\lambda_0\phi_0(z)\right) + \left(\frac{1}{2}\right)k_{tc}\left(\lambda_0\phi_0(z)\right)^2 + k_c\left(\mu_0^{II}\varphi_0^{II}(z)\right)\left\{\left(\lambda_0\phi_0(z)\right)\delta_{\text{theory, IRT}} + \left(\left[R_0\right]+z\left[R_1\right]+z^2\left[R_2\right]\right)\delta_{\text{theory, IRTO}}\right\} \quad (34)$$

*Bivariate pgf of order 0 of adduct radicals considering the length of each arm ($\varphi^{II}_{00}$):*

$$\frac{d}{dt}\left(\mu_{00}^{II}\varphi_{00}^{II}(z,w)\right) = k_a\left[\left(\mu_0^{I}\varphi_0^{I}(w)\right)\left(\lambda_0\phi_0(z)\right) + \left(\lambda_0\phi_0(w)\right)\left(\mu_0^{I}\varphi_0^{I}(z)\right)\right] - k_f\left(\mu_{00}^{II}\varphi_{00}^{II}(z,w)\right) - k_c\left\{\begin{array}{l}\lambda_0\left(\mu_{00}^{II}\varphi_{00}^{II}(z,w)\right)\delta_{\text{theory, IRT}} \\ +\left(\left[R_0\right]+\left[R_1\right]+\left[R_2\right]\right)\left(\mu_{00}^{II}\varphi_{00}^{II}(z,w)\right)\delta_{\text{theory, IRTO}}\end{array}\right\} \quad (35)$$

It can be noted that Equation (31) and (32) depend on the bivariate pgf of the adduct radical evaluated at $w = 1$. Taking into account that from the pgf definition given in Equation (29) $\varphi_0^I(w=1) = \phi(w=1) = 1$, applying this substitution into Equation (35) results in the expression shown in Equation (36).

*Bivariate pgf of order 0 of adduct radicals ($\varphi^{II}_{00}$) evaluated at w = 1:*

$$\frac{d}{dt}\left(\mu_{00}^{II}\varphi_{00}^{II}(z,1)\right) = k_a\left[\mu_0^{I}\left(\lambda_0\phi_0(z)\right) + \lambda_0\left(\mu_0^{I}\varphi_0^{I}(z)\right)\right] - k_f\left(\mu_{00}^{II}\varphi_{00}^{II}(z,1)\right) - k_c\left\{\lambda_0\left(\mu_{00}^{II}\varphi_{00}^{II}(z,1)\right)\delta_{\text{theory, IRT}} + \left(\left[R_0\right]+\left[R_1\right]+\left[R_2\right]\right)\left(\mu_{00}^{II}\varphi_{00}^{II}(z,1)\right)\delta_{\text{theory, IRTO}}\right\} \quad (36)$$

Besides, the pgf of the chain length distribution of the combination of all polymer species is needed in order to obtain this distribution. This pgf is defined as shown in Equation (37).

*Univariate pgf of order zero of the overall polymer ($R_n$ + $TR_n$ + $(RTR)_n$ + $P_n$) ($\Omega_0$):*

$$\Omega_0(z) = \frac{\lambda_0 \phi_0(z) + \mu_0^I \varphi_0^I(z) + \mu_0^{II} \varphi_0^{II}(z) + \varepsilon_0 \chi_0(z)}{\lambda_0 + \mu_0^I + \mu_0^{II} + \varepsilon_0} \quad (37)$$

Once these balances are solved the pgf are numerically inverted using appropriate numerical methods. Discrete points pertaining to the MWD are obtained as a result of this numerical inversion. Since the computation of each point is independent of any others, the accuracy of its prediction is unaffected by the number and location of the rest of the points. The number of points to be recovered must be set by the user considering that a large number will result in a smoother curve but a larger equation system. Additionally, in the case of univariate pgf inversion, the numerical method requires the user to specify a parameter *N*, which is the number of the terms of expansion of a polynomial.[45] As with any polynomial expansion, *N* needs to be large enough to provide good accuracy in the calculation of MWD, but small enough to avoid producing excessive noise due to error propagation and unnecessary enlargement of the system of equations. The same concept is extended to bivariate pgf inversion, for which two parameters, $N_1$ and $N_2$, need to be specified. The method for finding the optimal value of *N* has been reported elsewhere.[49] As was shown in that work, the MWD recovered from the pgf tends to converge to the true MWD as *N* approaches its optimal value, due to the greater accuracy of the numerical inversion. Based on this fact, the optimum *N* is selected by systematically increasing this parameter until there is no appreciable difference between the corresponding recovered distributions for two consecutive values. Therefore, the selection is performed based only on the MWDs recovered with different values of *N*. This fact makes it unnecessary to have any previous knowledge of the distribution in order to use the pgf technique.

Once the programmer sets the appropriate value of the parameters, the MWD is recovered by inverting the pgf transform without the need of any simplifying

assumptions or hypotheses. In addition, the mathematical model consists of a relatively small number of equations that can be solved in a reasonable time.

All the simulations were performed in gPROMS (Process Systems Enterprise, Ltd.). This equation-oriented modeling environment provides advanced solvers for steady-state and dynamic simulations or optimizations. In this work the proprietary solver DASOLV was used for the solution of mixed sets of differential and algebraic equations. DASOLV is based on variable time step/variable order backward differentiation formulae that has been proved to be efficient for a wide range of problems.[50] A standard desktop computer was used with an Intel® Core™2 Quad Q8400 2.66 GHz processor and 8 GB of RAM memory.

## 3. Results and Discussion

### 3.1. Accuracy of the Pgf Technique

In order to verify the reliability of the pgf technique, the MWDs predicted by the pgf model were compared with the ones resulting from the solution of the direct integration of the population balances. Since no simplifying assumptions were considered for the direct integration approach modeled in this work, the memory requirements to obtain the full bivariate MWD would be prohibitive on a standard desktop computer. Therefore, the comparison between the different approaches was performed only for the 1D distribution. To this end, Equation (21) for the total length of the two-arm adduct was used when the mass balances were integrated.

The MWDs obtained with the SF, IRT and IRTO theories are shown in Figure 1. The reference kinetic parameters shown in Table 1 were used. The same process conditions

were specified for all cases. For all the recovered 1D MWD reported in this work, values of $N$ of 18 or 19 were found to be optimal.

As previously reported, for these kinetic parameters the MWD predicted by the SF theory presents a bimodal shape.[16, 51] The small $k_f$ of the SF theory causes the population of the intermediate adduct species to be significant, leading to the high molecular weight peak of the bimodal MWD. The other peak of the MWD corresponds to the population of one-arm dormant chains. Conversely, in the cases of the IRT and IRTO theories the fragmentation of the intermediate adduct is fast and the concentration of this species is low. Therefore, only one peak corresponding to the one-arm dormant chain is observed in the MWD.

It can be seen that the points recovered by the pgf technique show good agreement with the curves corresponding to direct integration of the population balances. The pgf method was able to replicate properly both the width and the location of the MWD peaks, even for bimodal distributions, without any previous knowledge of the MWD shape.

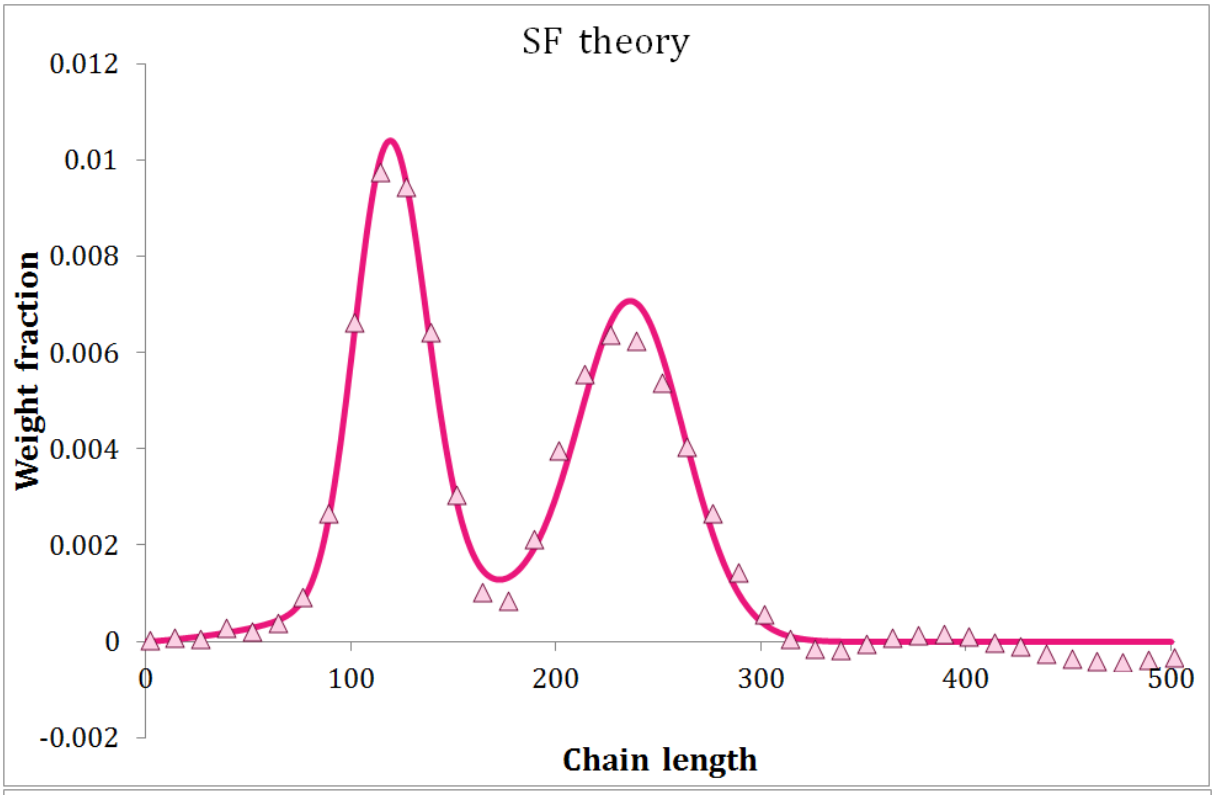
SF theory
0.012
0.01
0.008
0.006
0.004
0.002
0
-0.002
Weight fraction
0
100
200
300
400
500
Chain length

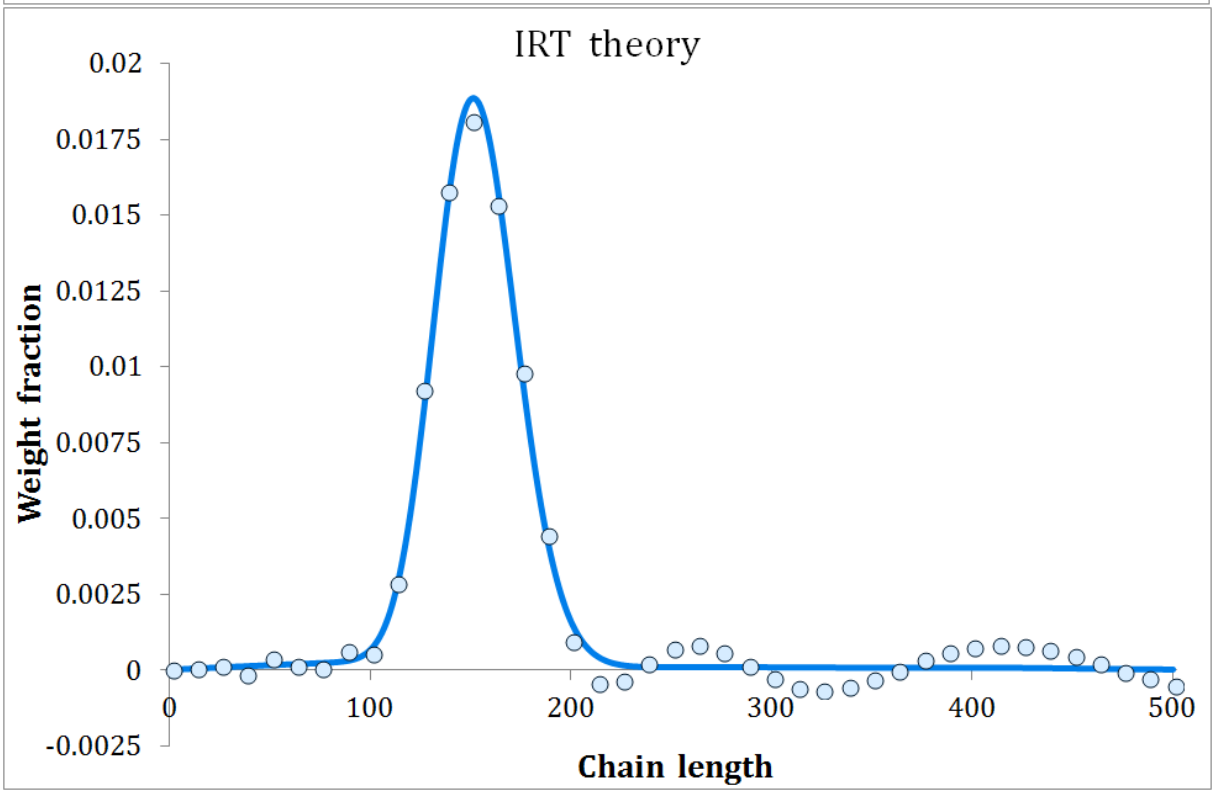
IRT theory
0.02
0.0175
0.015
0.0125
0.01
0.0075
0.005
0.0025
0
-0.0025
Weight fraction
0
100
200
300
400
500
Chain length

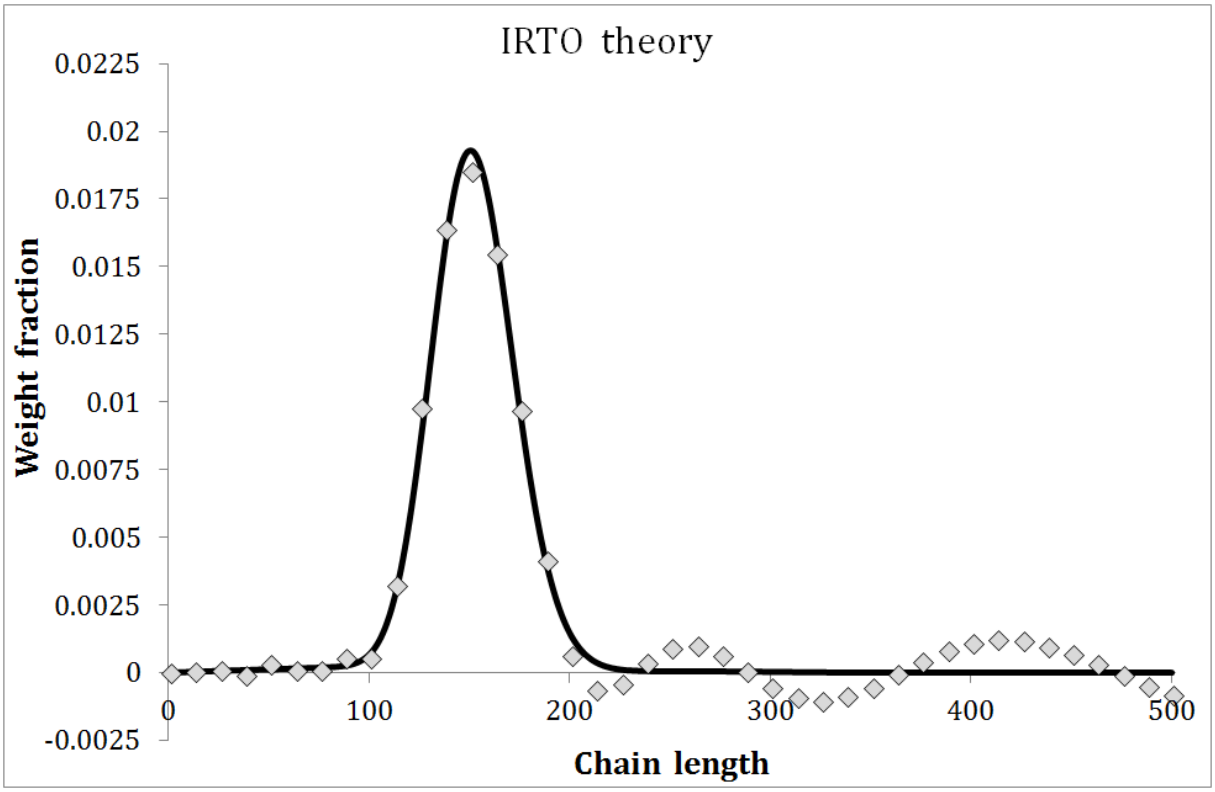


*Figure 1*. MWDs of the overall polymer obtained with the pgf technique and by direct integration. Process conditions: $[CTA]_0$ = 0.01 mol $L^{-1}$; $[I]_0$ = 0.005 mol $L^{-1}$; $[M]_0$ = 5 mol $L^{-1}$; 30% conversion. Solid lines = MWD by direct integration – Symbols = MWD points recovered with pgf technique.

Oscillations caused by numerical noise can be observed in the high molecular weight tail of the MWDs predicted by the pgf method. These oscillations do not belong to the actual MWD, but they could be mistakenly taken as a second peak of a bimodal MWD. Fortunately, the false peaks can be disregarded when recalculating the MWD with different values of the parameter *N*. As an example of the convergence of the MWDs when *N* approaches its optimum value, three curves obtained with different values of *N* are shown in Figure 2. In particular, for the case shown in this figure, the optimal *N* was found to be 19 since the difference between the MWDs recovered with *N*=18 (not shown here) and *N*=19 was minimal.

As was previously explained, in the region where the actual MWD lies, the recovered MWD curves for different values of *N* are similar as *N* approaches its optimum value. In the case shown in Figure 2, this is true up to a chain length of approximately 580 units.

At higher degrees of polymerization all the curves differ considerably from each other and show oscillations. This indicates that the oscillations are spurious, due to numerical noise propagation. In this way, numerical noise can be easily identified and neglected. In that case, the MWD is set to zero. This procedure was successfully used in previous works.[52, 53] The same concept applies to the inversion of the bivariate pgf.

The existence of this numerical error is a disadvantage of the pgf method since it makes it impossible to distinguish small shoulders on the high molecular weight tail. However, the main features of the MWD could still be properly predicted. Considering the small computational demands of this technique and the accuracy of its predictions, the error oscillations may be considered a minor drawback.

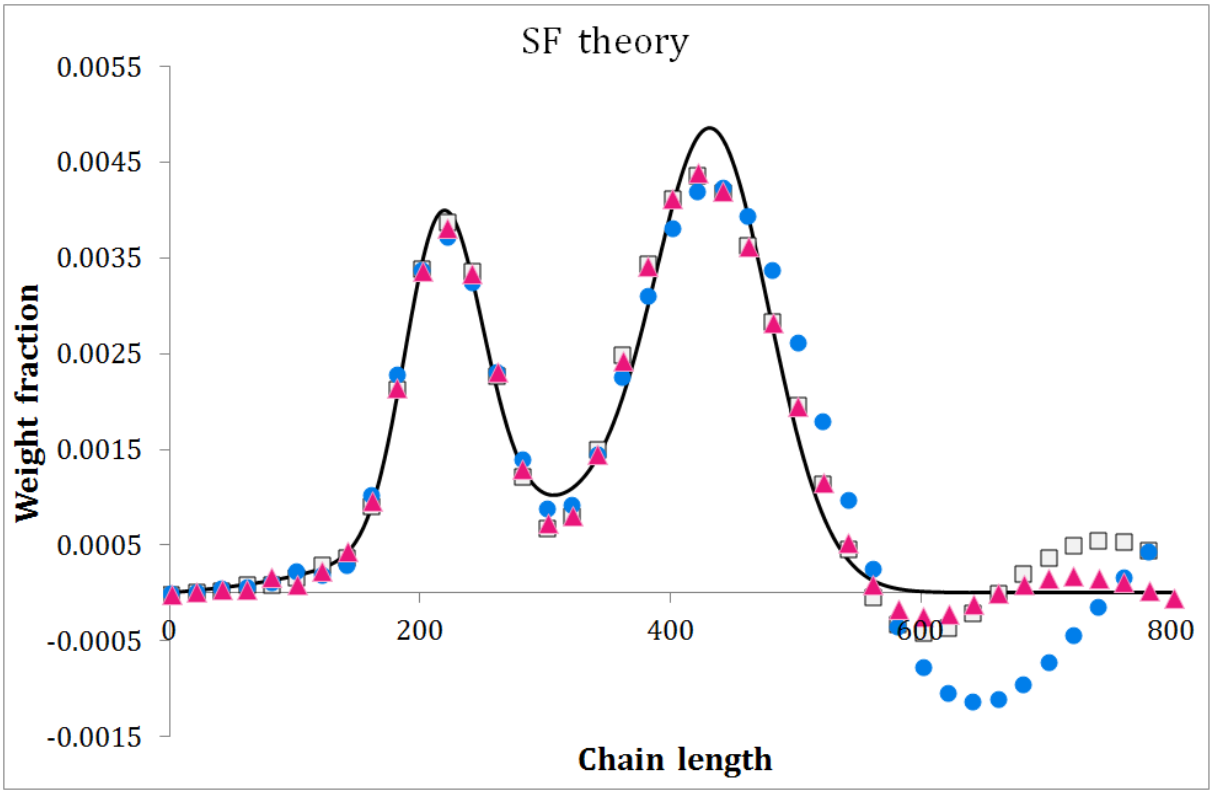


*Figure 2*. MWDs of the overall polymer obtained with the pgf technique and different values of parameter *N* of the pgf inversion method. Process conditions: $[CTA]_0$ = 0.01 mol $L^{-1}$; $[I]_0$ = 0.005 mol $L^{-1}$; $[M]_0$ = 5 mol $L^{-1}$; 30% conversion. — MWD by direct integration – Symbols: MWD points recovered with pgf technique and different *N* parameters: ● *N* = 14 - □ *N* = 17 - ▲ *N* = 19.

### 3.2. Efficiency of the pgf Technique

The differential algebraic equation (DAE) system associated with the pgf technique can be solved in a very short time. Several simulations were performed with different $[CTA]_0/[I]_0$ ratios, that lead to resins with diverse molecular weights. As a result the maximum chain length with nonzero values in the MWD varied. We call this the "maximum significant chain length." Table 2 shows how the computational time required to obtain the MWD both by direct integration of mass balances and by the pgf technique changes when considering physical systems of different molecular weights. It can be observed that it takes less time to solve the mathematical model when using the pgf method. Results are presented for the SF theory but similar information is obtained for the IRT and IRTO theories.

*Table 2*. CPU time required for computing the MWD by direct integration of the population balances and by the pgf method.

| *Max. chain length* | pgf technique | Direct integration |
|---|---|---|
| *250* | 6 s | 10 s |
| *350* | 6 s | 20 s |
| *500* | 5 s | 36 s |
| *600* | 6 s | 56 s |
| *800* | 6 s | 88 s |
| *1100* | 6 s | 193 s |
| *1850* | 6 s | 408 s |

In order to obtain the MWD from direct integration of the mass balances, an equation for each chain length from 1 up to the maximum significant length must be posed. Therefore, the size of the resulting DAE system increases for higher molecular weight polymers. On the contrary, the size of the DAE system for the pgf model depends on the number of points of the distribution curve that are computed and on the value of

parameter *N*, but not on the molecular weight of the polymer. For that reason, the difference in simulation time becomes more relevant as the molecular weight of the system increases. For this to be true, neither the value of *N* nor the number of MWD points computed should change significantly, but this is typically the case. Moreover, variations of *N* from 10 to 19 do not represent more than 3 seconds in computational time increment. It could be argued that smoothness of the MWD curve could be lost if the number of computed points is not increased as the molecular weight of the system increases, but this is not the case for the operating conditions considered in this work, as shown in Figure 3 for three of the MWD reported in Table 2. The results shown in Table 2 and in Figure 3 for the pgf method were obtained computing 40 points of the MWD in all cases with $N$ = 18 or 19.

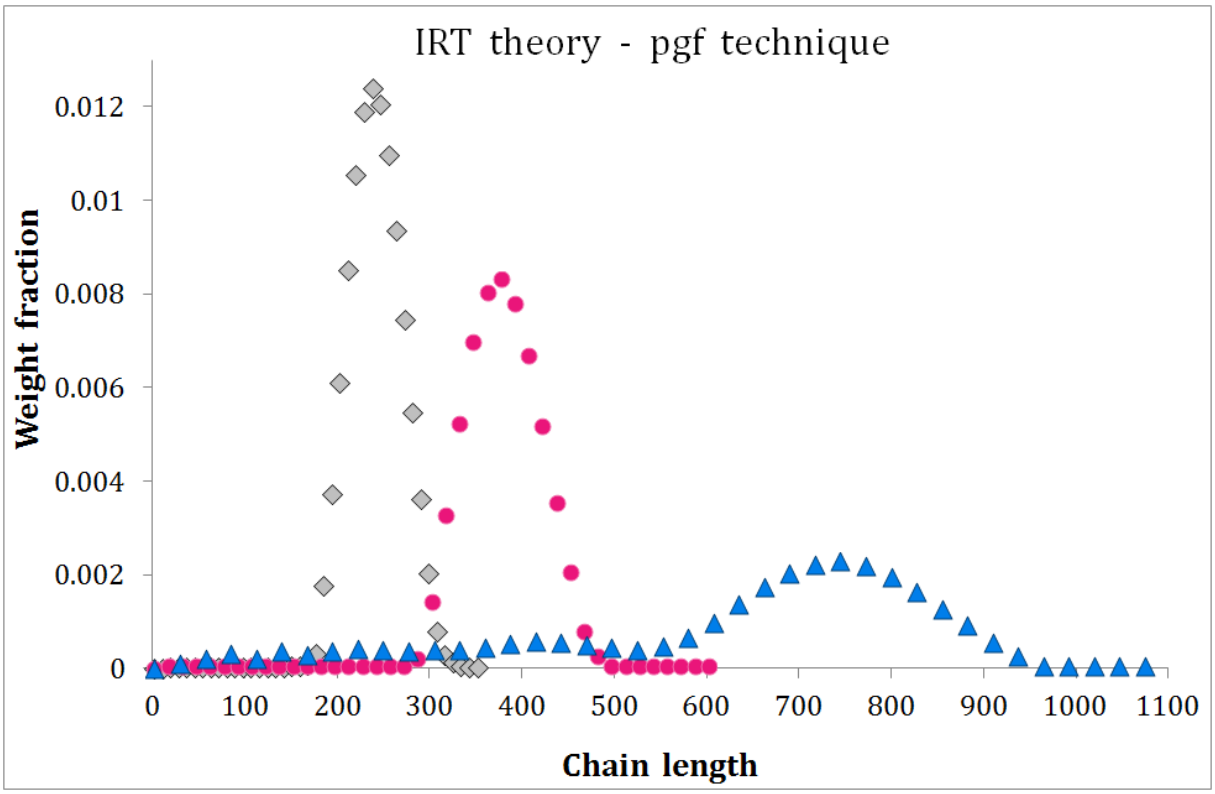


*Figure 3*. MWDs of the overall polymer obtained for the IRT theory kinetics with the pgf technique computing the same number of distribution points for systems of different molecular weight. ◇ $n_{max}$ = 350 units - ● $n_{max}$ = 600 units - ▲ $n_{max}$ = 1100 units.

The MWDs observed in Figure 3 were obtained with the conditions shown in Table 3.

*Table 3.* Conditions for runs presented in Figure 3.

| $n_{max}$ | $[M]_0$ mol $L^{-1}$ | $[I]_0$ mol $L^{-1}$ | $[CTA]_0$ mol $L^{-1}$ | Conversion % | Reaction time h |
|---|---|---|---|---|---|
| *350* | 5 | $8 \times 10^{-3}$ | $8 \times 10^{-3}$ | 37.9 | 2.871 |
| *600* | 5 | $1 \times 10^{-2}$ | $8 \times 10^{-3}$ | 58.9 | 4.871 |
| *1100* | 5 | $2.5 \times 10^{-2}$ | $6.5 \times 10^{-3}$ | 90.4 | 7.871 |

### 3.3. Bivariate MWD of the Two-Arm Adduct

The intermediate two-arm adduct $R_nTR_m$ is described by a two-dimensional distribution accounting for the chain lengths of each of its arms. A noteworthy feature of the mathematical model presented in this work is that it is able to provide a rigorous prediction of the full bivariate MWD of this intermediate. For this purpose, Equation (35) corresponding to the bivariate pgf of the two-arm adduct was used. It should be mentioned that the obtainment of the 2D MWD with the direct integration approach was prohibitive in terms of computational cost. Therefore, the obtained bivariate MWD are drawn only with the points recovered from the pgf balances. The numerical noise presented in the bivariate distribution was discarded as previously explained for the 1D distribution.

Figure 4 shows the MWD corresponding to the two-arm adduct for the SF theory. Process conditions are indicated in the figure caption. In this case, the optimum values of parameter *N* were found to be $N_1 = N_2 = 10$. This 2D distribution shows a notorious symmetry. It can be seen that the cross-sectional curves in planes $n=c$ (or $m=c$), where $c$ is a constant, have similar shapes for the various possible $c$ values. In fact, it can be verified that these curves differ only in a proportionality factor. Additionally, cross-sectional curves in planes perpendicular to the *m*-axis are analogous to the ones in planes perpendicular to the *n*-axis, and the maximum of the bivariate distribution is at

$n = m$ =210. These facts are consistent with the distributions of the two arms being independent of each other (i.e. $[R_nTR_m] = f(n,m) = f_1(n) \cdot f_2(m)$), and the individual distributions of each arm being the same ($f_1(n) \approx f_2(m)$). This is an expected result since any of the arms of the adduct experiences identical probabilities for any event of the reaction mechanism. Symmetry with respect to the line $m = n$ is also observed, which is logical since $R_nTR_m$ is the same moiety as $R_mTR_n$. Equivalent results are observed for different operating conditions and for the other two RAFT kinetic mechanisms. Another example may be found in the Supporting Information.

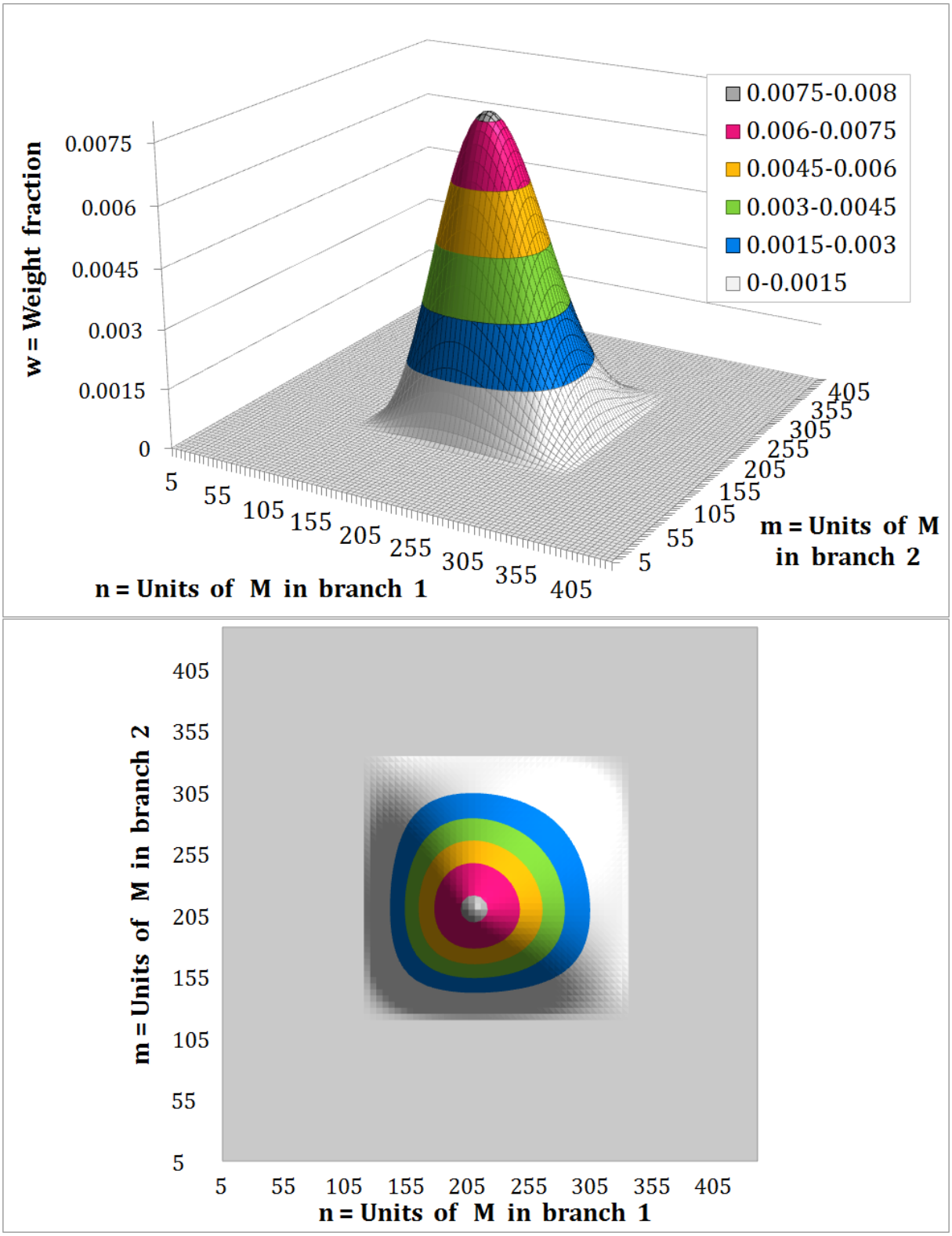


*Figure 4*. Bivariate MWD of the intermediate adduct obtained with the pgf technique for SF theory kinetics. Process conditions: $[CTA]_0$ = 0.005 mol $L^{-1}$; $[I]_0$ = 0.005 mol $L^{-1}$; $[M]_0$ = 5 mol $L^{-1}$; 30% conversion.

### 3.4. Sensitivity analysis

As shown previously, the pgf technique is a reliable and efficient method for obtaining the MWD of RAFT polymers. Therefore, a sensitivity study on rate constants was performed using this method aiming at showcasing its versatility. The MWD shown from now on are drawn from the recovered points of the pgf, with removal of the numerical error oscillations. For all cases, the optimal *N* parameters were found to be either 18 or 19. A generic monomeric unit with molecular weight of 100 g $mol^{-1}$ was considered.

The effect of changes in rate constants was evaluated at two different process conditions, shown in Table 4.

*Table 4*. Common conditions for simulations.

| **Condition 1:** | **Condition 2:** |
|---|---|
| $[M]_0$ = 5 mol $L^{-1}$ | $[M]_0$ = 5 mol $L^{-1}$ |
| $[CTA]_0$ = 5 x $10^{-3}$ mol $L^{-1}$ | $[CTA]_0$ = 1 x $10^{-2}$ mol $L^{-1}$ |
| $[I]_0$ = 5 x $10^{-3}$ mol·$L^{-1}$ | $[I]_0$ = 5 x $10^{-3}$ mol·$L^{-1}$ |
| Final conversion = 30% | Final conversion = 30% |

**Fragmentation Rate Constant ($k_f$) in the SF Theory**

The SF theory assumes that the retardation effect observed in RAFT processes is due to the slow fragmentation of the two-arm adduct. Therefore, it leads to fragmentation rate constants much lower than the ones used for the IRT or IRTO theories. It turns out that an accurate value of this rate constant is very important in the SF theory. For the rate constants considered in this work the equilibrium constant ($K_{eq} = k_f/k_a$) is equal to $10^{-8}$. This small value leads to a bimodal behavior of the distribution. Figure 5 shows the resulting MWD of the overall polymer species when the reference value of $k_f$ in the SF theory is changed in ±50%. The weight fractions of one-arm dormant (TR) and two-arm

adduct (RTR) molecules are reported in the figure pointing to their corresponding peaks. Taking into consideration that the only species present are TR, RTR, propagating radicals and terminated polymer, and that the fraction of propagating radicals is in the order of $10^{-6}$, the weight fraction of terminated polymer may be calculated from the information in the figure.

For the two reaction conditions shown in this figure, it can be seen that when increasing $k_f$ the height of the second peaks decreases and the one of the first peak increases. This is expected and was already reported by other authors.[16] A higher $k_f$ would indicate a faster fragmentation of the two-arm adduct which would cause a larger concentration of one-arm dormant chains.

As expected, for each of the conditions shown in Figure 5, the number average molecular weight is the same for all values of $k_f$ ($\overline{Mn}$ ~ 29800 g mol$^{-1}$ when $[CTA]_0 = 5 \times 10^{-3}$ mol L$^{-1}$, and $\overline{Mn}$ ~ 15000 g mol$^{-1}$ for $[CTA]_0 = 1 \times 10^{-2}$ mol L$^{-1}$). This is so because the number of reacted monomers does not vary (equal conversion), nor does the total number of chains, which is equal to the initial concentration of transfer agent according to the SF theory. However, it can be observed in Figure 5 that the chain lengths of the populations of both one-arm dormant chains and intermediate two-arm adduct are larger for higher $k_f$. This fact can be explained as a redistribution of the same number of reacted monomers in a larger proportion of shorter chains (one arm dormant chains), with respect to the longer intermediate adduct (twice the length of the one arm moiety). The number average molecular weight remains the same because the number of shorter chains is larger. Note that this analysis would not have been possible without knowledge of the full MWD.

It can also be seen from the times required to reach the 30% conversion (Rx time), that $k_f$ also influences the polymerization rate. Higher values of this rate constant increase

the rate of reaction, since more active radicals are released that can propagate with monomers. This is expected and has been reported by other authors.[16, 34]

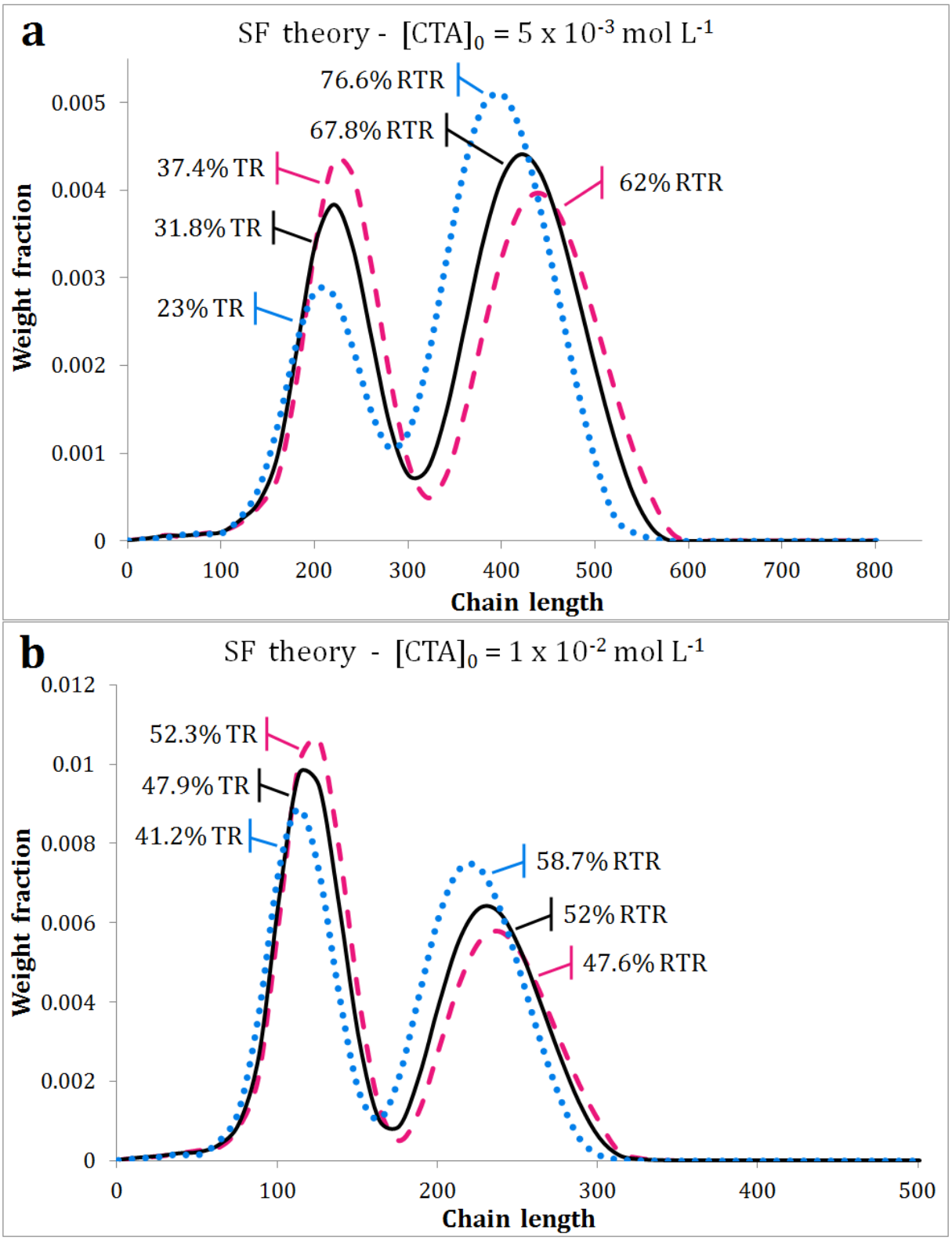


*Figure 5.* Effect changing the fragmentation constant $k_f$ by 50% on the MWD of the overall polymer and polymerization rate according to the SF kinetics.

a) $[CTA]_0 = 5 \times 10^{-3}$ mol $L^{-1}$: – – $1.5 \times k_{f\,ref}$ (Rx time = 17.3 h) ——— $k_{f\,ref}$ (Rx time = 20.7 h) • • • $0.5 \times k_{f\,ref}$ (Rx time = 27.8 h).
b) $[CTA]_0 = 1 \times 10^{-2}$ mol $L^{-1}$: – – $1.5 \times k_{f\,ref}$ (Rx time = 27.7 h) ——— $k_{f\,ref}$ (Rx time = 34.2 h) • • • $0.5 \times k_{f\,ref}$ (Rx time = 49.8 h).

The features mentioned above are observed for each of both reaction conditions. Differences between them can be found in the polymerization rate and the molecular weight range. For the higher CTA content, polymerization rate and molecular weights are lower. This is a typical behavior of RAFT systems and has been reported elsewhere.[24, 39, 51] In addition, the proportion of one-arm dormant chains with respect to the intermediate adduct is higher.

In all of these cases the chain growth is well controlled given that bimolecular termination is reduced to a minimum. As a result the fraction of dead polymer is less than 1%, and all chains grow at the same speed on average, resulting in very low polydispersity indexes (between 1.14 and 1.18).

The effect of more significant changes in $k_f$ on the MWD and polymerization rate, of two orders of magnitude in the reference value of this kinetic constant, is shown in Figure 6. It should be mentioned that the same behavior described before with respect to MWD and reaction rate is observed in this figure. In the extreme case of increasing $k_f$ by a factor of 100, the $K_{eq}$ ceases being so small and the growth of the TR peak and the reduction of the RTR peak leads to a monomodal MWD. The small weight fractions of RTR reported in Figure 6 are imperceptible as a peak in the MWD curves. These distributions are similar to the ones that are obtained by the IRT theory with the reference rate constants, which were included in the figure for the sake of comparison. This result is expected since when the fragmentation constant increases so significantly, the "slow fragmentation" ceases being slow, and only a small percentage of chains are in the form of the two arms adduct. This is so even though the values of $k_f$ of the SF and IRT theories still differ by 4 orders of magnitude.

It is interesting to note what happens when the same constant is diminished by a factor of 100. For the lower $[CTA]_0$, the height of the TR peak decreases so much with respect to the one corresponding to RTR chains, that is overlapped by the RTR peak and the resulting MWD is also unimodal. On the other hand, for the higher $[CTA]_0$ the MWD remains bimodal because the content of TR chains is larger.

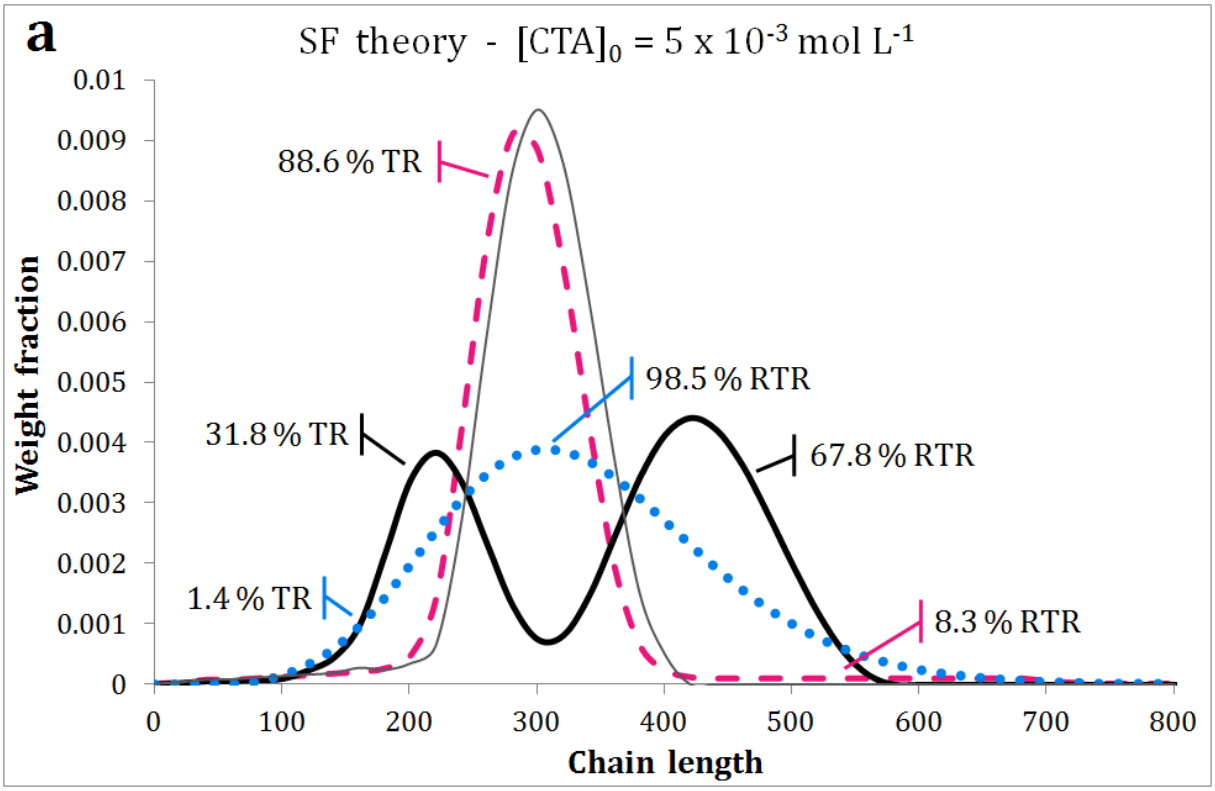

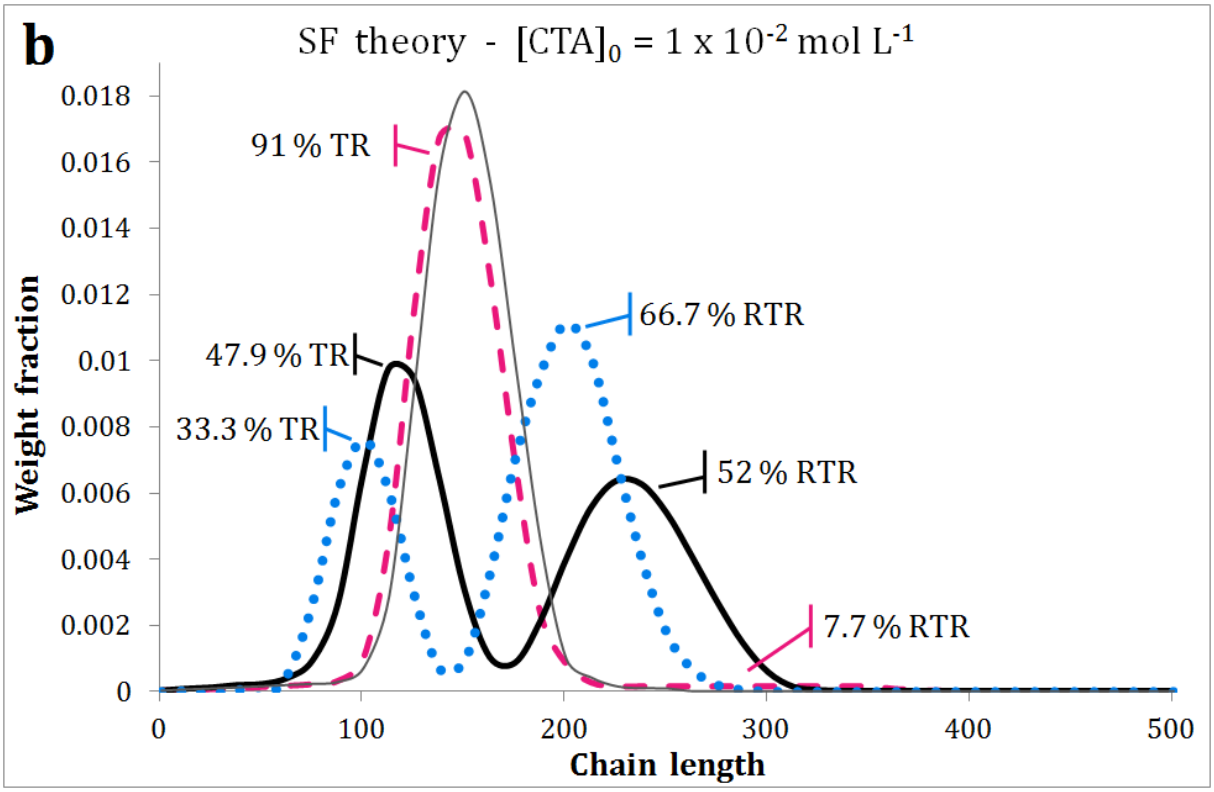


*Figure 6*. Effect of changing the fragmentation constant $k_f$ by two orders of magnitude on the MWD of the overall polymer and the polymerization rate according to the SF kinetics.

a) $[CTA]_0 = 5 \times 10^{-3}$ mol $L^{-1}$: — IRT theory $k_{f\,ref}$ – – 100 × $k_{f\,ref}$ (Rx time = 2.9 h) — $k_{f\,ref}$ (Rx time = 20.7 h) • • • 0.01 × $k_{f\,ref}$ (Rx time = 103.3 h).

b) $[CTA]_0 = 1 \times 10^{-2}$ mol $L^{-1}$: — IRT theory $k_{f\,ref}$ – – 100 × $k_{f\,ref}$ (Rx time = 3.8 h) — $k_{f\,ref}$ (Rx time = 34.2 h) • • • 0.01 × $k_{f\,ref}$ (Rx time = 1027.5 h).

**Fragmentation Rate Constant ($k_f$) and Cross-Termination Rate Constant ($k_c$) in the IRT and IRTO Theories**

The IRT and IRTO theories consider that the fragmentation reaction of the intermediate two-arm adduct is fast, and incorporate a cross-termination reaction between the adduct and active radicals. Figure 7 and 8 show mathematical model outputs for changes in kinetic constants of these reactions within ±2 orders of magnitude with respect to their reference values in the IRT theory. Unlike the SF theory, substantial changes are noticeable only when $k_f$ is reduced in 2 orders of magnitude or $k_c$ is increased in the same amount. This suggests that there is a threshold value for this constants beyond which changes in their values are not very significant.

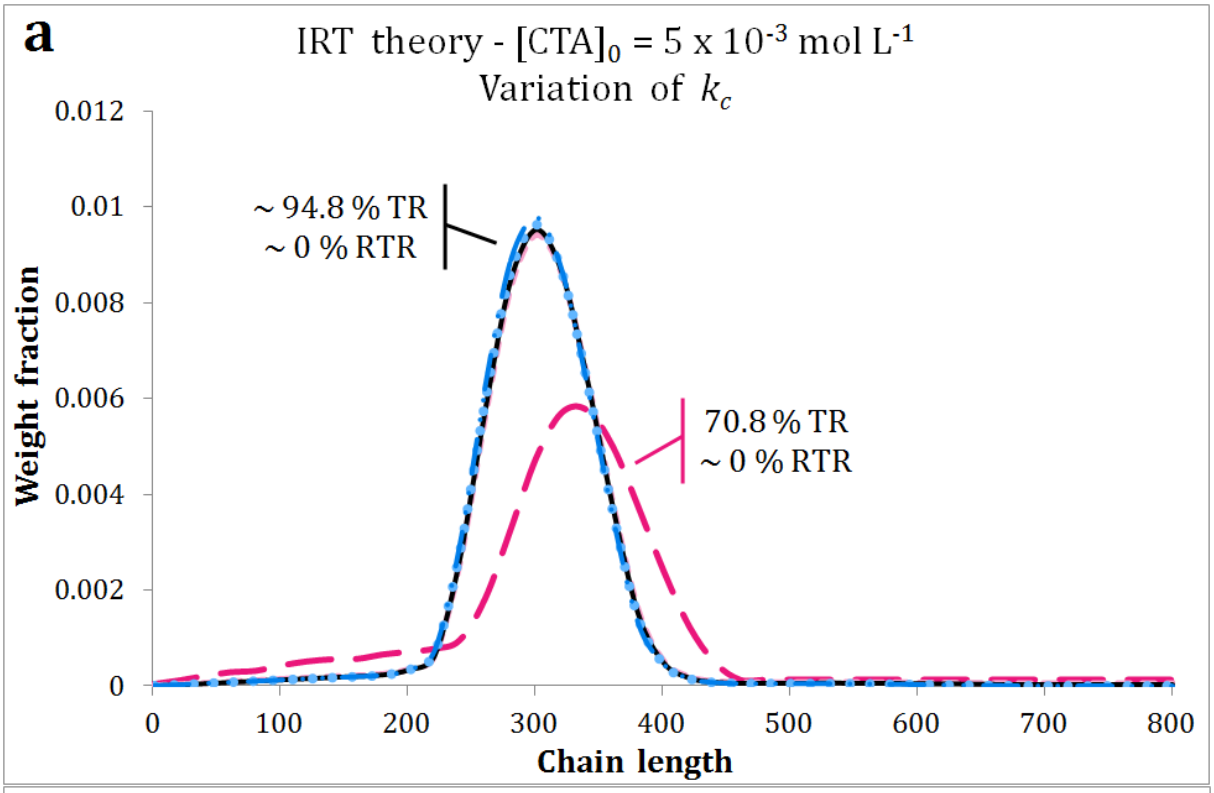


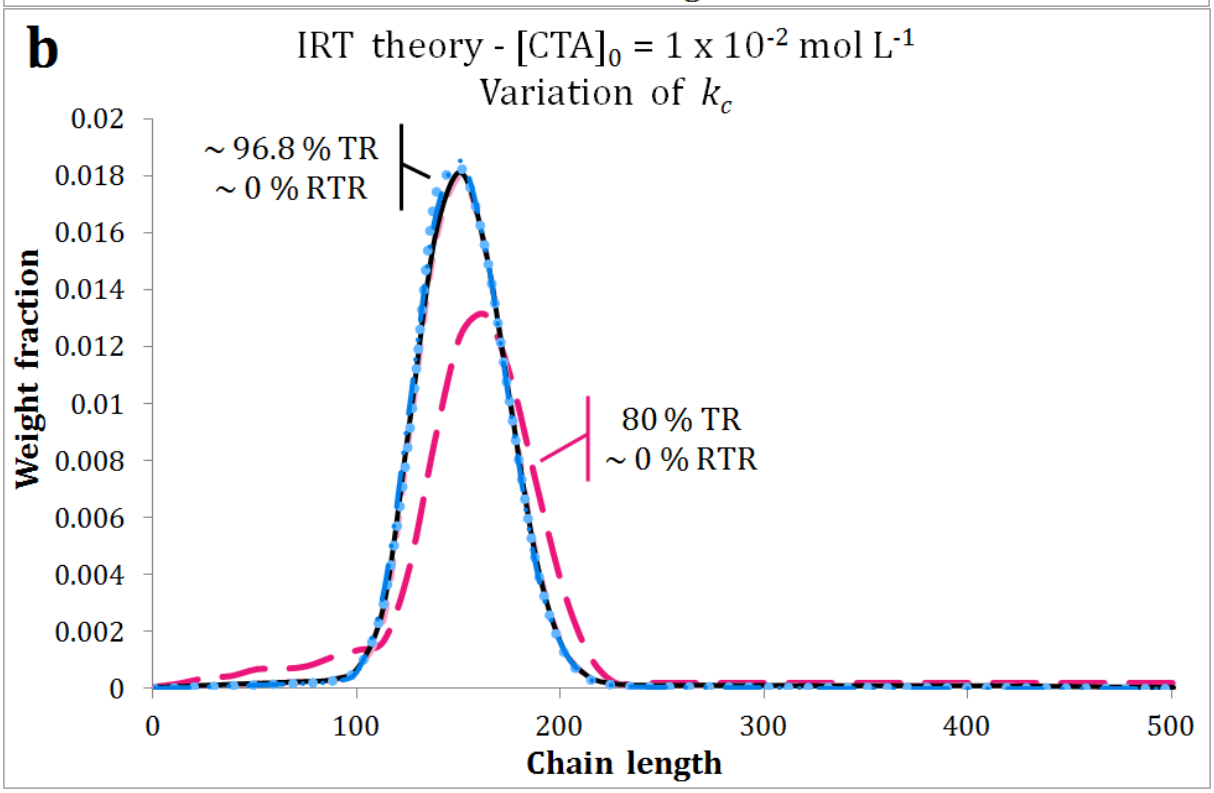


*Figure 7*. Effect of the cross-termination constant $k_c$ on the MWD of the overall polymer and the polymerization rate according to the IRT theory.

a) $[CTA]_0 = 5 \times 10^{-3}$ mol $L^{-1}$: — — $100 \times k_{c\,ref}$ (Rx time = 15.27 h) — — $1.5 \times k_{c\,ref}$ (Rx time = 2.68 h) ——— $k_{c\,ref}$ (Rx time = 2.48 h) • • • $0.5 \times k_{c\,ref}$ (Rx time = 2.26 h) —·—·— $0.01 \times k_{c\,ref}$ (Rx time = 2.02 h).

b) $[CTA]_0 = 1 \times 10^{-2}$ mol $L^{-1}$: — — $100 \times k_{c\,ref}$ (Rx time = 23.46 h) — — $1.5 \times k_{c\,ref}$ (Rx time = 3.22 h) ——— $k_{c\,ref}$ (Rx time = 2.87 h) • • • $0.5 \times k_{c\,ref}$ (Rx time = 2.48 h) —·—·— $0.01 \times k_{c\,ref}$ (Rx time = 2.03 h).

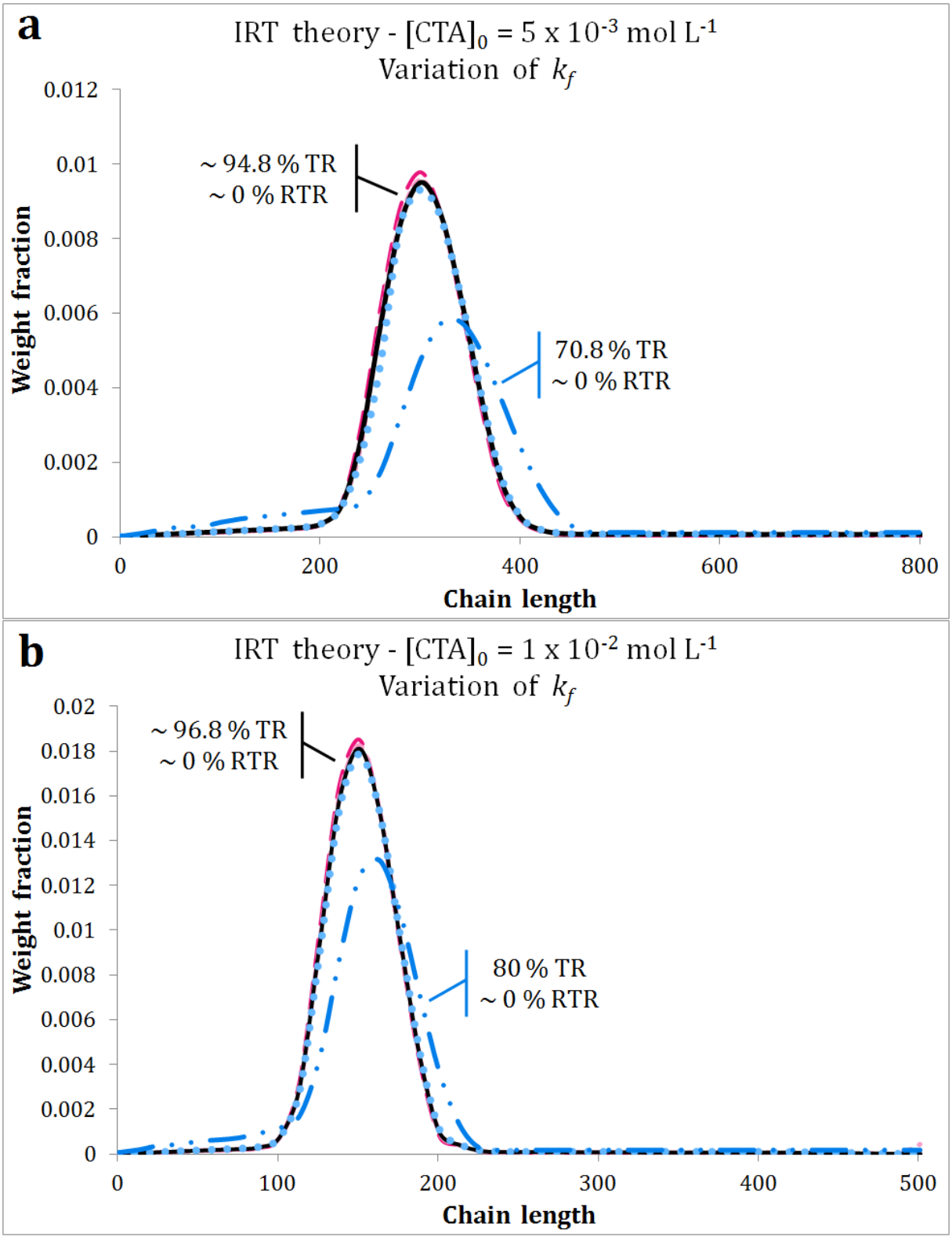


*Figure 8.* Effect of the fragmentation constant $k_f$ on the MWD of the overall polymer and the polymerization rate according to the IRT theory.

a) $[CTA]_0 = 5 \times 10^{-3}$ mol $L^{-1}$: — — $100 \times k_{f\,ref}$ (Rx time = 2.02 h) — — $1.5 \times k_{f\,ref}$ (Rx time = 2.33 h) ——— $k_{f\,ref}$ (Rx time = 2.48 h) • • • $0.5 \times k_{f\,ref}$ (Rx time = 2.87 h) —·—·— $0.01 \times k_{f\,ref}$ (Rx time = 15.28 h).

b) $[CTA]_0 = 1 \times 10^{-2}$ mol $L^{-1}$: — — $100 \times k_{f\,ref}$ (Rx time = 2.03 h) — — $1.5 \times k_{f\,ref}$ (Rx time = 2.62 h) ——— $k_{f\,ref}$ (Rx time = 2.87 h) • • • $0.5 \times k_{f\,ref}$ (Rx time = 3.53 h)

— · · — $0.01 \times k_{f\,ref}$ (Rx time = 23.47 h).

In both cases, variations in the system outputs can be attributed to the higher probability that the two-arm adduct cross-terminates with active radicals.

It can be seen from the reaction times required to achieve the 30% conversion shown in Figure 7, that when the cross-termination rate constant is increased the polymerization rate decreases. This is due to the reduction in the concentration of active radicals because of the faster termination reaction with the two-arm intermediate adduct. The fraction of terminated polymer rises because of a higher concentration of the three-arm stars, product of the cross-termination reaction.

Figure 8 shows that an analogous effect to the increase in $k_c$ in 2 orders of magnitude is observed when the fragmentation rate constant is reduced in the same proportion. In this case, cross-termination competes favorably with fragmentation, and a large amount of three-arm polymer is produced at the expense of a negligible amount of RTR. Actually, the effect of an increase in $k_c$ or a decrease in $k_f$ on the population of chains is very similar. To illustrate this point, Figure 9 shows the evolution with conversion of the one-arm dormant chains (TR), linear terminated chains (P), and three-arm star terminated chains (star P). Please recall that P molecules are the result of the termination reaction between active radicals as shown in Equation (7) and (8). For the sake of clarity, only the curves corresponding to $k_{ref}$, $0.01 \times k_{f\,ref}$, and $100 \times k_{c\,ref}$ are shown. It can be seen that the curves corresponding to the increase in $k_c$ overlap with the ones corresponding to the decrease in $k_f$. Besides, it can be noticed that the three-arm star polymer constitute nearly all the dead polymer chains in the reaction medium for the highest $k_c$ or the lowest $k_f$ values.

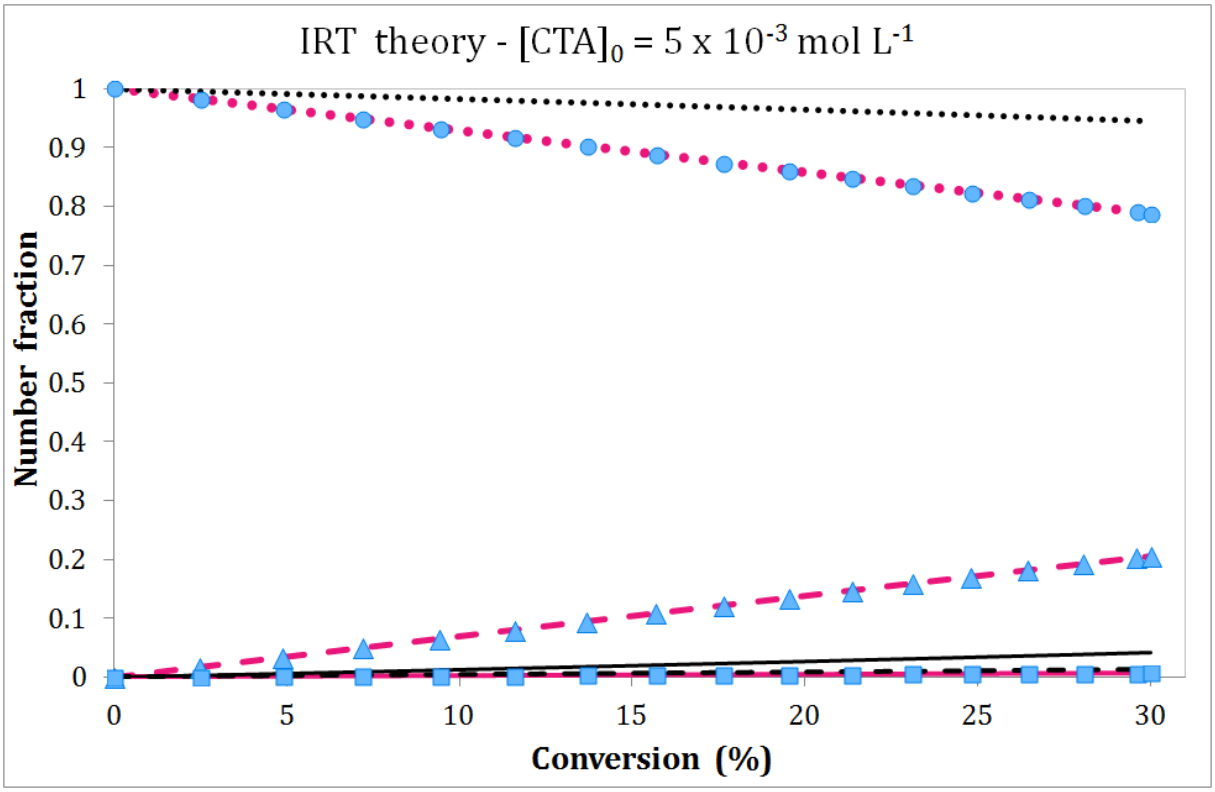


*Figure 9.* Comparison of the number fraction of the dead polymer species when $k_c$ is increased or $k_f$ is diminished in 2 orders of magnitude with respect to the reference value. ••• 100 × $k_{c\,ref}$ - TR – – – 100 × $k_{c\,ref}$ - star P ——— 100 × $k_{c\,ref}$ – P •••• $k_{ref}$ - TR – – – $k_{ref}$ - star P ——— $k_{ref}$ - P ● 0.01 × $k_{f\,ref}$ - TR ▲ 0.01 × $k_{f\,ref}$ - star P ■ 0.01 × $k_{f\,ref}$ - P

On the other hand, changes in $k_f$ or $k_c$ do not affect significantly the predicted MWD or the polymerization rate when using the IRTO theory. It was verified that the MWD does not vary perceptibly even when rate constants varying in 4 orders of magnitude were used for $[CTA]_0 = 5\times10^{-3}$ mol·L$^{-1}$ or $[CTA]_0 = 1\times10^{-2}$ mol·L$^{-1}$. Examples are shown in the Supporting Information.

The influence of $k_f$ and $k_c$ observed for the IRT theory is not observed in the IRTO theory because only oligomeric radicals, with very low concentration in the reaction medium, take place in the cross-termination reaction.

## 4. Conclusions

A mathematical model was presented that may successfully simulate the RAFT polymerization according to either the SF, IRT or IRTO kinetics making use of the pgf transform technique. The model allows obtaining the full MWD accurately using small computational resources regardless of the molecular weight of the product. No previous knowledge of the shape of the distribution is required. Spurious oscillations are observed in the high molecular weight tail of the MWD that can be easily recognized and discarded. It is shown in this work that this minor drawback may be counterbalanced by the multiple advantages of the pgf technique. The bivariate distribution corresponding to the two-arm intermediate adduct is also obtained. This distribution allows getting insights into the characteristics of this species.

A sensitivity analysis was performed on several of the kinetic constants to study the behavior of the system, showing that the pgf technique is a valuable tool for modeling and studying many complex kinetic mechanisms. The results agreed with those reported in the existing literature,[16, 34] and showed that the value of the fragmentation constant $k_f$ is critical for the SF theory. For the IRT theory, both the fragmentation constant $k_f$ and cross-termination constant $k_c$ are important, but there is a threshold value beyond which the model becomes insensitive to further changes. The IRTO theory showed little sensitivity to the values of both rate constants.

## Nomenclature

| | |
|---|---|
| $f$ | initiator efficiency |
| $[I]$ | concentration of initiator |
| $k_i$ | kinetic constant of generic reaction $i$ |

| | |
|---|---|
| $[M]$ | concentration of monomer |
| $\overline{Mn_i}$ | number average molecular weight of generic species *i* |
| MWD | weight average molecular weight distribution |
| $[P_n]$ | concentration of terminated polymer with *n* units of M |
| $[R_n]$ | concentration of radical chain with *n* units of M |
| $[R_nTR_s]$ | concentration of two-arm adduct (intermediate radical) with *n* units of M in one branch and *s* units in the other branch |
| $[(RTR)_n]$ | concentration of two-arm adduct with total length of *n* units of M |
| $[TR_n]$ | concentration of dormant radical of one arm with *n* units of M |
| *w* | Second dummy variable for pgf |
| *z* | First dummy variable for pgf |

## Greek Symbols

| | |
|---|---|
| $\delta_{n,a}$ | Kronecker delta |
| $\mu_a^I$ | *a*th order moment of one-arm dormant |
| $\mu_a^{II}$ | *a*th, *b*th order moment of two-arm adduct considering its total length |
| $\mu_{a,b}^{II}$ | *a*th, *b*th order moment of two-arm adduct considering each branch length |
| $d\mu_{0\ n}^{II}$ | Parcial moment of the two-arm intermediate adduct |
| $\lambda_a$ | *a*th order moment of macroradical chain |
| $\varepsilon_a$ | *a*th order moment of terminated copolymer |

$\phi_0(z)$ *0*th order probability generating function of radical chain

$\varphi_0^I(z)$ *0*th order pgf of dormant chain of one-arm

$\varphi_0^{II}(z)$ *0*th order pgf of two–arm intermediate adduct

$\varphi_{00}^{II}(z,w)$ *0*th order bivariate pgf of two-arm adduct radicals

$\varphi_{00}^{II}(z,1)$ *0*th order bivariate pgf of two-arm adduct radicals evaluated at $w = 1$

$\chi_0(z)$ *0*th order pgf of terminated polymer

$\Omega_0(z)$ *0*th order pgf of the overall polymer

## Supporting Information

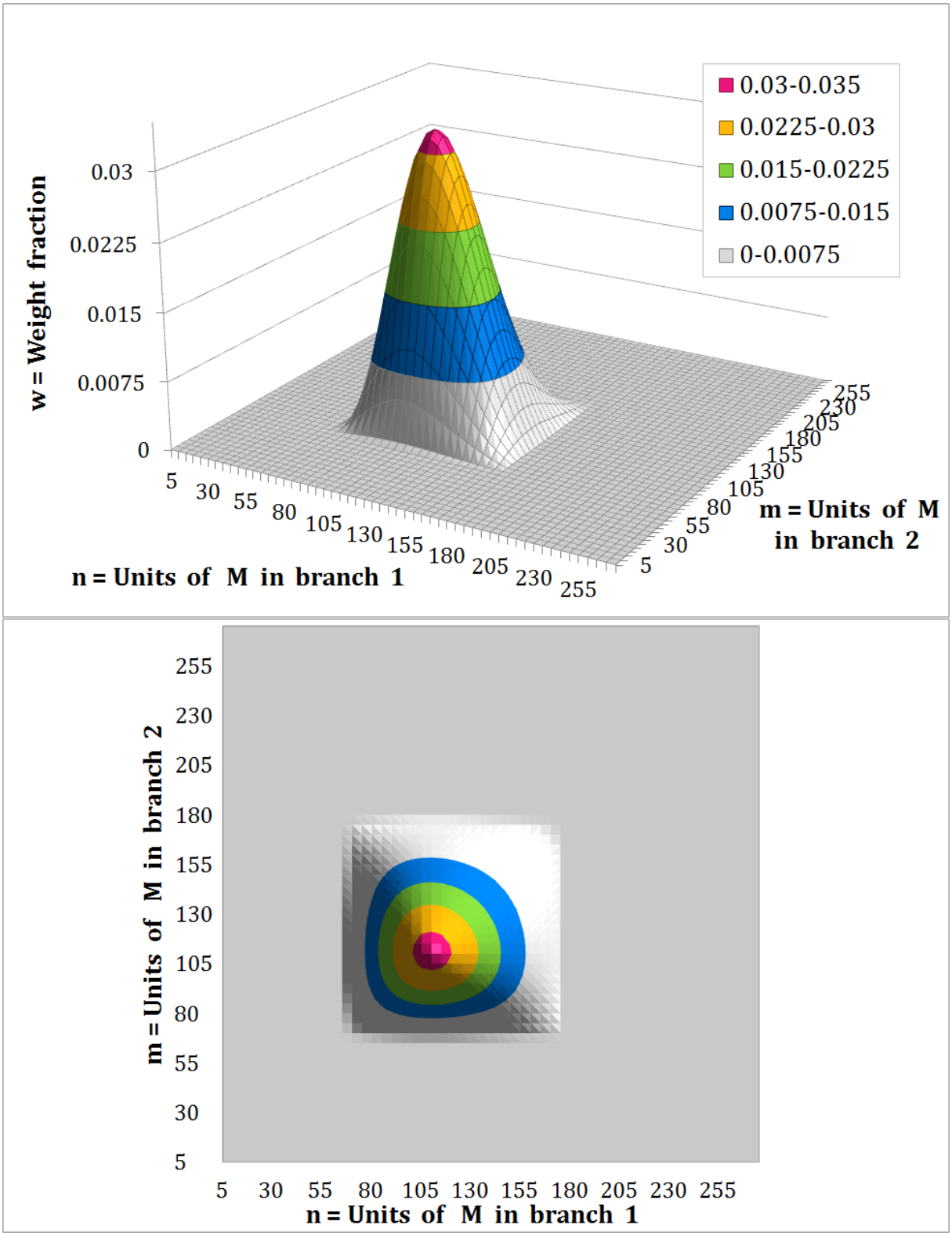


Bivariate MWD of the intermediate adduct obtained with the pgf technique for IRT theory kinetics. Process conditions: $[CTA]_0$ = 0.01 mol $L^{-1}$; $[I]_0$ = 0.005 mol $L^{-1}$; $[M]_0$ = 5 mol $L^{-1}$; 30% conversion.

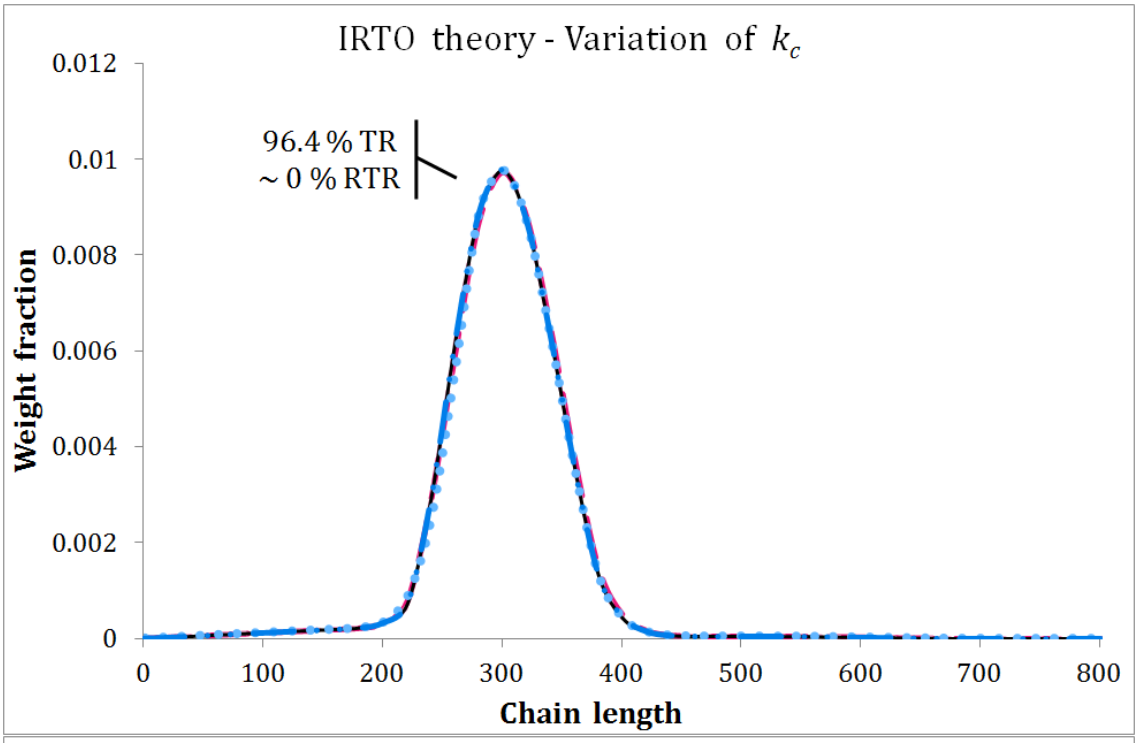


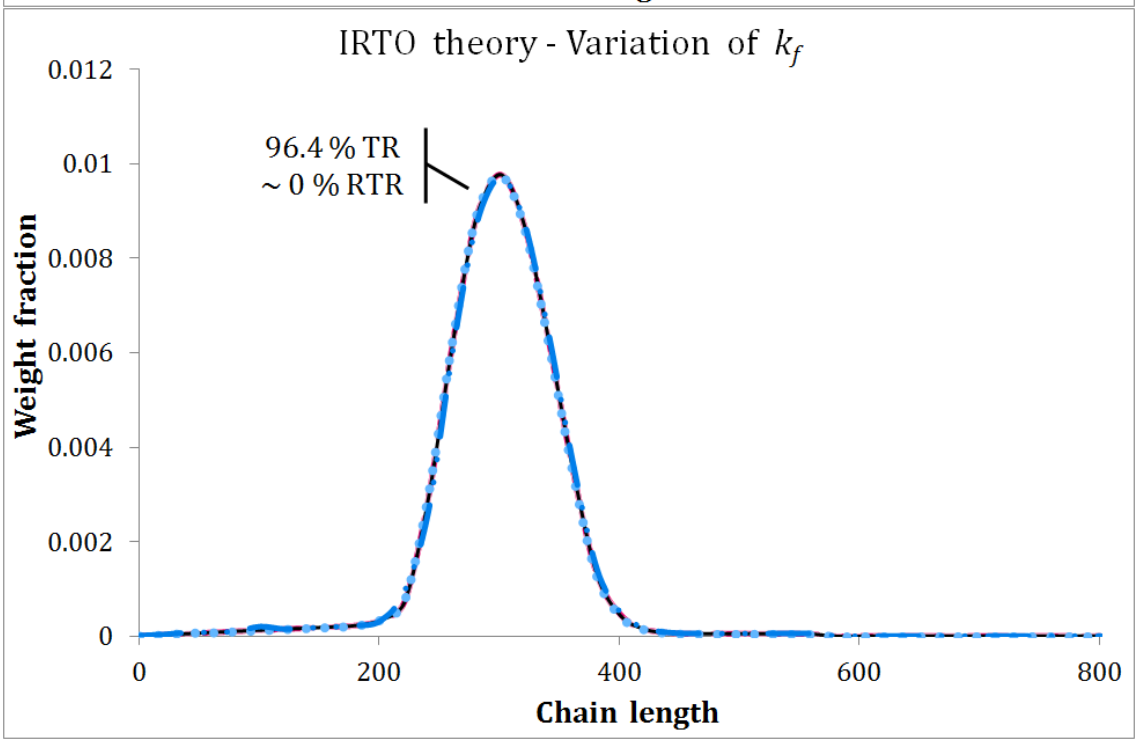


Effect of the fragmentation constant $k_f$ and of the cross-termination constant $k_c$ on the MWD of the overall polymer and the polymerization rate according to the IRTO theory for $[CTA]_0 = 5 \times 10^{-3}$ mol $L^{-1}$.

a) Variation of $k_f$: 100 x $k_{f\,ref}$ (Rx time = 2.02 h) 1.5 x $k_{f\,ref}$ (Rx time = 2.02 h) $k_{f\,ref}$ (Rx time = 2.02 h) 0.5 x $k_{f\,ref}$ (Rx time = 2.03 h) 0.01 x $k_{f\,ref}$ (Rx time = 2.24 h).

b) Variation of $k_c$: 100 x $k_{c\,ref}$ (Rx time = 2.23 h) 1.5 x $k_{c\,ref}$ (Rx time = 2.03 h) $k_{c\,ref}$ (Rx time = 2.02 h) 0.5 x $k_{c\,ref}$ (Rx time = 2.02 h) 0.01 x $k_{c\,ref}$ (Rx time = 2.02 h).

Acknowledgements: The authors acknowledge the financial support of CONICET (National Research Council of Argentina), ANPCyT (National Agency for Promotion of Science and Technology of Argentina), and UNS (Universidad Nacional del Sur).

Keywords: modeling, molecular weight distribution, pgf, reversible addition fragmentation chain transfer (RAFT)

## References

[1] K. Matyjaszewski, K. A. Davis, *Statistical, Gradient, Block and Graft Copolymers by Controlled/Living Radical Polymerizations*, Springer-Verlag, Berlin, Germany, 1st edition, **2002**.

[2] D. Konkolewicz, B. S. Hawkett, A. Gray-Weale, S. Perrier, *Macromolecules* **2008**, *41*, 6400.

[3] M. Zhang, W. H. Ray, *Ind. Eng. Chem. Res.* **2001**, *40*, 4336.

[4] J. Liu, L. Tao, J. Xu, Z. Jia, C. Boyer, T. P. Davis, *Polymer* **2009**, *50*, 4455.

[5] A. Sogabe, C. L. McCormick, *Macromolecules* **2009**, *42*, 5043.

[6] O. I. Strube, G. Schmidt-Naake, *Macromol. Symp.* **2009**, *275-276*, 13.

[7] D. Wang, X. Li, W. J. Wang, X. Gong, B. G. Li, S. Zhu, *Macromolecules* **2012**, *45*, 28.

[8] W. A. Braunecker, K. Matyjaszewski, *Prog. Polym. Sci.* **2007**, *32*, 93.

[9] B. Klumperman, E. T. A. Van Den Dungen, J. P. A. Heuts, M. J. Monteiro, *Macromol. Rapid Commun.* **2010**, *31*, 1846.

[10] I. S. Altarawneh, M. Srour, V. G. Gomes, *Polymer - Plastics Technology and Engineering* **2007**, *46*, 1103.

[11] C. Barner-Kowollik, M. Buback, B. Charleux, M. L. Coote, M. Drache, T. Fukuda, A. Goto, B. Klumperman, A. B. Lowe, J. B. McLeary, G. Moad, M. J. Monteiro, R. D. Sanderson, M. P. Tonge, P. Vana, *J. Polym. Sci., Part A: Polym. Chem.* **2006**, *44*, 5809.

[12] M. Buback, O. Janssen, R. Oswald, S. Schmatz, P. Vana, *Macromol. Symp.* **2007**, *248*, 158.

[13] M. Drache, G. Schmidt-Naake, M. Buback, P. Vana, *Polymer* **2005**, *46*, 8483.

[14] Y. Luo, R. Wang, L. Yang, B. Yu, B. Li, S. Zhu, *Macromolecules* **2006**, *39*, 1328.

[15] H. Tobita, *Macromol. Theory Simul.* **2013**, *22*, 399.

[16] I. Zapata-González, E. Saldívar-Guerra, J. Ortiz-Cisneros, *Macromol. Theory Simul.* **2011**, *20*, 370.

[17] D. I. Zhou, X. Zhu, J. Zhu, H. Yin, *J. Polym. Sci., Part A: Polym. Chem.* **2005**, *43*, 4849.

[18] C. Barner-Kowollik, J. F. Quinn, D. R. Morsley, T. P. Davis, *J. Polym. Sci., Part A: Polym. Chem.* **2001**, *39*, 1353.

[19] D. Konkolewicz, B. S. Hawkett, A. Gray-Weale, S. Perkier, *J. Polym. Sci., Part A: Polym. Chem.* **2009**, *47*, 3455.

[20] M. J. Monteiro, H. De Brouwer, *Macromolecules* **2001**, *34*, 349.

[21] W. Meiser, M. Buback, *Macromol. Rapid Commun.* **2012**, *33*, 1273.

[22] G. Moad, *Macromolecular Chemistry and Physics* **2014**, *215*, 9.

[23] R. Wang, Y. Luo, B. Li, X. Sun, S. Zhu, *Macromol. Theory Simul.* **2006**, *15*, 356.

[24] H. Tobita, *Macromol. React. Eng.* **2010**, *4*, 643.

[25] K. Suzuki, Y. Kanematsu, T. Miura, M. Minami, S. Satoh, H. Tobita, *Macromol.*

*Theory Simul.* **2014**, *23*, 136.

[26] S. R. S. Ting, T. P. Davis, P. B. Zetterlund, *Macromolecules* **2011**, *44*, 4187.

[27] M. Zhang, W. H. Ray, *J. Appl. Polym. Sci.* **2002**, *86*, 1047.

[28] A. R. Wang, S. Zhu, *J. Polym. Sci., Part A: Polym. Chem.* **2003**, *41*, 1553.

[29] A. R. Wang, S. Zhu, *Macromol. Theory Simul.* **2003**, *12*, 663.

[30] A. R. Wang, S. Zhu, *Macromol. Theory Simul.* **2003**, *12*, 196.

[31] Y. Ye, F. J. Schork, *Ind. Eng. Chem. Res.* **2009**, *48*, 10827.

[32] A. Feldermann, M. L. Coote, M. H. Stenzel, T. P. Davis, C. Barner-Kowollik, *J. Am. Chem. Soc.* **2004**, *126*, 15915.

[33] J. Pallares, G. Jaramillo-Soto, C. Flores-Cataño, E. V. Lima, L. M. F. Lona, A. Penlidis, *J. Macromol. Sci., Pure Appl. Chem.* **2006**, *43*, 1293.

[34] C. Barner-Kowollik, J. F. Quinn, T. L. U. Nguyen, J. P. A. Heuts, T. P. Davis, *Macromolecules* **2001**, *34*, 7849.

[35] A. R. Wang, S. Zhu, Y. Kwak, A. Goto, T. Fukuda, M. S. Monteiro, *J. Polym. Sci., Part A: Polym. Chem.* **2003**, *41*, 2833.

[36] M. Wulkow, M. Busch, T. P. Davis, C. Barner-Kowollik, *J. Polym. Sci., Part A: Polym. Chem.* **2004**, *42*, 1441.

[37] I. Zapata-González, E. Saldívar-Guerra, A. Flores-Tlacuahuac, E. Vivaldo-Lima, J. Ortiz-Cisneros, *Can. J. Chem. Eng.* **2012**, *90*, 804.

[38] M. Wulkow, *Macromol. React. Eng.* **2008**, *2*, 461.

[39] D. Konkolewicz, M. Siauw, A. Gray-Weale, B. S. Hawkett, S. Perrier, *J. Phys. Chem. B* **2009**, *113*, 7086.

[40] H. Tobita, *Macromol. React. Eng.* **2008**, *2*, 371.

[41] S. W. Prescott, *Macromolecules* **2003**, *36*, 9608.

[42] S. W. Prescott, M. J. Ballard, E. Rizzardo, R. G. Gilbert, *Macromol. Theory*

*Simul.* **2006**, *15*, 70.

[43] H. Chaffey-Millar, D. Stewart, M. M. T. Chakravarty, G. Keller, C. Barner-Kowollik, *Macromol. Theory Simul.* **2007**, *16*, 575.

[44] C. Fortunatti, C. Sarmoria, A. Brandolin, M. Asteasuain, *Comput. Chem. Eng.* **2014**, *66*, 214.

[45] M. Asteasuain, A. Brandolin, *Macromol. Theory Simul.* **2010**, *19*, 342.

[46] C. Sarmoria, M. Asteasuain, A. Brandolin, *Can. J. Chem. Eng.* **2012**, *90*, 263.

[47] M. Asteasuain, C. Sarmoria, A. Brandolin, *Polymer* **2002**, *43*, 2513.

[48] A. Brandolin, M. Asteasuain, *Macromol. Theory Simul.* **2013**, *22*, 273.

[49] M. Asteasuain, A. Brandolin, C. Sarmoria, *Polymer* **2002**, *43*, 2529.

[50] *gPROMS v3.7 - Model Developer Guide*, Process Systems Enterprise Ltd., London, UK, **2013**.

[51] C. Fortunatti, C. Sarmoria, A. Brandolin, M. Asteasuain, *Comput. Chem. Eng.* **2014**, doi: 10.1016/j.compchemeng.2014.02.017.

[52] M. Asteasuain, S. Matheus, M. K. Lenzi, R. A. Hutchinson, M. Cunningham, A. Brandolin, J. C. Pinto, C. Sarmoria, *Macromol. React. Eng.* **2007**, *1*, 622.

[53] M. Asteasuain, C. Sarmoria, A. Brandolin, *J. Appl. Polym. Sci.* **2003**, *88*, 1676.

## Figure Captions

*Figure 1*. MWDs of the overall polymer obtained with the pgf technique and by direct integration. Process conditions: $[CTA]_0$ = 0.01 mol $L^{-1}$; $[I]_0$ = 0.005 mol $L^{-1}$; $[M]_0$ = 5 mol $L^{-1}$; 30% conversion. Solid lines = MWD by direct integration – Symbols = MWD points recovered with pgf technique.

*Figure 2*. MWDs of the overall polymer obtained with the pgf technique and different values of parameter *N* of the pgf inversion method. Process conditions: $[CTA]_0$ = 0.01 mol $L^{-1}$; $[I]_0$ = 0.005 mol $L^{-1}$; $[M]_0$ = 5 mol $L^{-1}$; 30% conversion. — MWD by direct integration – Symbols: MWD points recovered with pgf technique and different *N* parameters: ● *N* = 14 - □ *N* = 17 - ▲ *N* = 19.

*Figure 3*. MWDs of the overall polymer obtained for the IRT theory kinetics with the pgf technique computing the same number of distribution points for systems of different molecular weight. ◈ $n_{max}$ = 350 units - ● $n_{max}$ = 600 units - ▲ $n_{max}$ = 1100 units.

*Figure 4*. Bivariate MWD of the intermediate adduct obtained with the pgf technique for SF theory kinetics. Process conditions: $[CTA]_0$ = 0.005 mol $L^{-1}$; $[I]_0$ = 0.005 mol $L^{-1}$; $[M]_0$ = 5 mol $L^{-1}$; 30% conversion.

*Figure 5*. Effect changing the fragmentation constant $k_f$ by 50% on the MWD of the overall polymer and polymerization rate according to the SF kinetics.

c) $[CTA]_0 = 5 \times 10^{-3}$ mol $L^{-1}$: – – 1.5 × $k_{f\,ref}$ (Rx time = 17.3 h) — $k_{f\,ref}$ (Rx time = 20.7 h) • • • 0.5 × $k_{f\,ref}$ (Rx time = 27.8 h).

d) $[CTA]_0 = 1 \times 10^{-2}$ mol $L^{-1}$: – – 1.5 × $k_{f\,ref}$ (Rx time = 27.7 h) — $k_{f\,ref}$ (Rx time = 34.2 h) • • • 0.5 × $k_{f\,ref}$ (Rx time = 49.8 h).

*Figure 6*. Effect of changing the fragmentation constant $k_f$ by two orders of magnitude on the MWD of the overall polymer and the polymerization rate according to the SF kinetics.

c) $[CTA]_0 = 5 \times 10^{-3}$ mol $L^{-1}$: — IRT theory $k_{f\,ref}$ – – 100 × $k_{f\,ref}$ (Rx time = 2.9 h) — $k_{f\,ref}$ (Rx time = 20.7 h) • • • 0.01 × $k_{f\,ref}$ (Rx time = 103.3 h).

d) $[CTA]_0 = 1 \times 10^{-2}$ mol $L^{-1}$: — IRT theory $k_{f\,ref}$ – – 100 × $k_{f\,ref}$ (Rx time = 3.8 h) — $k_{f\,ref}$ (Rx time = 34.2 h) • • • 0.01 × $k_{f\,ref}$ (Rx time = 1027.5 h).

*Figure 7.* Effect of the cross-termination constant $k_c$ on the MWD of the overall polymer and the polymerization rate according to the IRT theory.

c) $[CTA]_0 = 5 \times 10^{-3}$ mol $L^{-1}$: $100 \times k_{c\,ref}$ (Rx time = 15.27 h) $1.5 \times k_{c\,ref}$ (Rx time = 2.68 h) $k_{c\,ref}$ (Rx time = 2.48 h) $0.5 \times k_{c\,ref}$ (Rx time = 2.26 h) $0.01 \times k_{c\,ref}$ (Rx time = 2.02 h).

d) $[CTA]_0 = 1 \times 10^{-2}$ mol $L^{-1}$: $100 \times k_{c\,ref}$ (Rx time = 23.46 h) $1.5 \times k_{c\,ref}$ (Rx time = 3.22 h) $k_{c\,ref}$ (Rx time = 2.87 h) $0.5 \times k_{c\,ref}$ (Rx time = 2.48 h) $0.01 \times k_{c\,ref}$ (Rx time = 2.03 h).

*Figure 8.* Effect of the fragmentation constant $k_f$ on the MWD of the overall polymer and the polymerization rate according to the IRT theory.

c) $[CTA]_0 = 5 \times 10^{-3}$ mol $L^{-1}$: $100 \times k_{f\,ref}$ (Rx time = 2.02 h) $1.5 \times k_{f\,ref}$ (Rx time = 2.33 h) $k_{f\,ref}$ (Rx time = 2.48 h) $0.5 \times k_{f\,ref}$ (Rx time = 2.87 h) $0.01 \times k_{f\,ref}$ (Rx time = 15.28 h).

d) $[CTA]_0 = 1 \times 10^{-2}$ mol $L^{-1}$: $100 \times k_{f\,ref}$ (Rx time = 2.03 h) $1.5 \times k_{f\,ref}$ (Rx time = 2.62 h) $k_{f\,ref}$ (Rx time = 2.87 h) $0.5 \times k_{f\,ref}$ (Rx time = 3.53 h) $0.01 \times k_{f\,ref}$ (Rx time = 23.47 h).

*Figure 9.* Comparison of the number fraction of the dead polymer species when $k_c$ is increased or $k_f$ is diminished in 2 orders of magnitude with respect to the reference value. $100 \times k_{c\,ref}$ - TR $100 \times k_{c\,ref}$ - star P $100 \times k_{c\,ref}$ – P $k_{ref}$ - TR $k_{ref}$ - star P $k_{ref}$ - P 0.01 × $k_{f\,ref}$ - TR 0.01 × $k_{f\,ref}$ - star P 0.01 × $k_{f\,ref}$ - P

*Table of Content*

Cecilia Fortunatti,* Claudia Sarmoria, Adriana Brandolin, Mariano Asteasuain

**Modeling of RAFT Polymerization using Probability Generating Functions. Detailed Prediction of Full Molecular Weight Distributions and Sensitivity Analysis**

**A model based on the pgf transform is presented that simulates the RAFT polymerization according to any of the three main kinetic mechanisms discussed in the literature.** The full MWD and the bivariate distribution corresponding to the two-arm intermediate adduct are obtained. A sensitivity analysis over several of the kinetic constants is also performed.

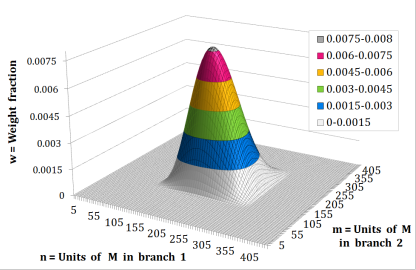

Click here to download Supporting Information: Supporting Information.docx

Click here to download Production Data: Figure 1.docx

Click here to download Production Data: Figure 2.docx

Click here to download Production Data: Figure 3.docx

Click here to download Production Data: Figure 4.docx

Click here to download Production Data: Figure 5.docx

Click here to download Production Data: Figure 6.docx

Click here to download Production Data: Figure 7.docx

Click here to download Production Data: Figure 8.docx

Click here to download Production Data: Figure 9.docx

Click here to download Production Data: Full article.docx